

Non-Coherent Over-the-Air Decentralized Stochastic Gradient Descent

Nicolò Michelusi

Abstract—This paper proposes a Decentralized Stochastic Gradient Descent (DSGD) algorithm to solve distributed machine-learning tasks over wirelessly-connected systems, without the coordination of a base station. It combines local stochastic gradient descent steps with a Non-Coherent Over-The-Air (NCOTA) consensus scheme at the receivers, that enables concurrent transmissions by leveraging the waveform superposition properties of the wireless channels. With NCOTA, local optimization signals are mapped to a mixture of orthogonal preamble sequences, and transmitted concurrently over the wireless channel under half-duplex constraints. Consensus is estimated by non-coherently combining the received signals with the preamble sequences and mitigating the impact of noise and fading via a consensus step-size. NCOTA-DSGD operates without channel state information (typically used in over-the-air computation schemes for channel inversion) and leverages the channel pathloss to mix signals, without explicit knowledge of the mixing weights (typically known in consensus-based optimization). It is shown that, with a suitable tuning of decreasing consensus and learning stepsizes, the error (measured as Euclidean distance) between the local and globally optimum models vanishes with rate $\mathcal{O}(k^{-1/4})$ after k iterations. NCOTA-DSGD is evaluated numerically by solving an image classification task on the MNIST dataset, cast as a regularized cross-entropy loss minimization. Numerical results depict faster convergence vis-à-vis running time than implementations of the classical DSGD algorithm over digital and analog orthogonal channels, when the number of learning devices is large, under stringent delay constraints.

I. INTRODUCTION

The advent of networks constituted of a massive number of devices with sensing, computation and wireless communication capabilities opens up new opportunities in the design of large-scale machine learning (ML) applications. Yet, leveraging the enormous amount of data generated by these devices brings new challenges, associated with the decentralized nature of the system and resource-limited wireless connectivity. *Federated learning* (FL) [2] has emerged as a new paradigm to alleviate the communication burden and privacy concerns associated with the transmission of raw data to a ML server. It enables N spatially distributed devices with local datasets generated from their embedded sensors to cooperatively learn a global ML model, solution of

$$\mathbf{w}^* = \arg \min_{\mathbf{w} \in \mathbb{R}^d} \underbrace{\frac{1}{N} \sum_{i=1}^N f_i(\mathbf{w})}_{\triangleq F(\mathbf{w})}. \quad (\text{P})$$

Here, $f_i(\mathbf{w}) = \frac{1}{|\mathcal{D}_i|} \sum_{\xi \in \mathcal{D}_i} \phi(\xi; \mathbf{w})$ is a local function only known to node i , representing the empirical loss over its local dataset \mathcal{D}_i , with loss function $\phi(\xi; \mathbf{w})$ computed on the

d datapoint ξ ; \mathbf{w} is a d -dimensional parameter vector, so that $F(\mathbf{w})$ is the network-wide empirical loss.

Conventional FL aims at solving (P) based on a client-server architecture, where the N edge devices (the clients) interact with a parameter server (PS, such as a base station) over multiple rounds, by mimicking the updates of a centralized stochastic gradient descent (SGD) algorithm [3]: at round k , the PS *broadcasts* the current model \mathbf{w}_k ; upon receiving \mathbf{w}_k , each node *computes* a stochastic gradient (based on a minibatch $\mathcal{B}_{i,k}$) $\mathbf{g}_{i,k} = \frac{1}{|\mathcal{B}_{i,k}|} \sum_{\xi \in \mathcal{B}_{i,k}} \nabla \phi(\xi; \mathbf{w}_k)$, and *communicates* it back to the PS; the latter finally *aggregates* the local gradients and updates the model as $\mathbf{w}_{k+1} = \mathbf{w}_k - \eta_k \frac{1}{N} \sum_i \mathbf{g}_{i,k}$, with learning stepsize η_k . Despite its simplicity, such client-server architecture of FL encounters several challenges in wireless environments: 1) devices far away from the PS (e.g., in rural environments), may be unable to communicate reliably, due to severe pathloss conditions [4]; 2) uplink communications to the PS may be a severe bottleneck when N is large, due to bandwidth constraints [3]; 3) in case of failure of the PS, the entire system may break down. Therefore, in many important scenarios, such as those characterized by large number of edge devices spread over a large geographical area, a decentralized communication and learning architecture may be more attractive: in this setting, edge devices communicate to each other without the aid of a central coordinator [5].

Schemes solving (P) in decentralized architectures have been extensively studied in the research community [6]. For instance, consider the popular *decentralized gradient descent* (DGD) protocol [7], [8], and its stochastic gradient variant (DSGD) [9]: each node (i), at round k , transmits $\mathbf{w}_{i,k}$ to its neighbors in the network; upon receiving the signals from all its neighbors, it then updates its local state via consensus, followed by a local gradient step,

$$\mathbf{w}_{i,k+1} = \mathbf{w}_{i,k} + \sum_{j=1}^N \omega_{i,j} (\mathbf{w}_{j,k} - \mathbf{w}_{i,k}) - \eta_k \mathbf{g}_{i,k}, \quad (1)$$

where $\mathbb{E}[\mathbf{g}_{i,k}] = \nabla f_i(\mathbf{w}_{i,k})$. In the above equation, ω are non-negative mixing weights such that $\omega_{i,j} = \omega_{j,i}$ and $\sum_j \omega_{i,j} = 1$, consistent with the network connectivity (i.e., $\omega_{i,j} = 0$ if nodes i and j are not neighbors of each other). Yet, executing (1) inherently assumes communications over orthogonal, noise-free links (represented by a mesh network), and relies on a predetermined set of weights ω to aggregate the incoming signals. In many practical scenarios, such as swarms of UAVs, the N nodes communicate with each other over wireless links, subject to various impairments: interference from concurrent transmissions, fading and noise may preclude the ability of node i to receive error-free copies of its neighbors' signals. Mitigating these sources of errors may require: {1} a centralized coordinator responsible for careful

N. Michelusi is with the School of Electrical, Computer and Energy Engineering, Arizona State University.

Part of this work has been submitted to IEEE ICC 2023 [1].

This research has been funded in part by NSF under grant CNS-2129615.

network scheduling and interference management $\{2\}$ channel state information (CSI) to compensate signal fluctuations and link outages caused by fading. However, such centralized coordination may be a source of severe overhead, and CSI acquisition may be impaired by pilot contamination [10].

These challenges call for the design of decentralized optimization schemes capable of operating over (and leveraging properties of) wireless channels. In this paper, we develop a *Non-Coherent (NC)-Over-the-Air (OTA)-DSGD* algorithm, that implements DSGD over wireless channels subject to noise, fading and interference. NCOTA-DSGD enables non-coherent concurrent transmissions from multiple nodes, and allows to directly estimate the consensus step $\sum_j \omega_{i,j}(\mathbf{w}_{j,k} - \mathbf{w}_{i,k})$ of (1) by leveraging the waveform superposition properties of the wireless channels, without the need for CSI nor for direct knowledge of the mixing weights. While OTA-based schemes developed under centralized [4], [11]–[17] and decentralized [18]–[20] FL architectures rely on accurate CSI and power control at the transmitters to compensate signal fluctuations due to fading, NCOTA-DSGD overcomes these limitations by encoding the transmitted signals via a set of orthogonal preamble sequences (inspired by the preamble-based technique developed in [21] for centralized FL), coupled with non-coherent combining at the receivers. While decentralized FL works [18]–[20] rely on prior knowledge of the mixing weights, NCOTA-DSGD exploits the structure of the large-scale pathloss coefficients, without their explicit knowledge. We prove that, with a suitable design of decreasing *consensus* and *learning* stepsizes, the error (Euclidean distance) between the local models and the global solution of (P) decays to zero with rate $\mathcal{O}(k^{-1/4})$, thus improving the state-of-the-art [18], [19] exhibiting a non-vanishing error gap.

A. Related work

The study of distributed optimization algorithms to solve (P) is vast and can be traced back to the seminal work [22]. Compression schemes are developed in [23]–[25], and finite-bit quantization schemes are developed in [26]–[29]. These works allow decentralized algorithms to operate over finite capacity channels, under errors induced by compression and/or quantization of the signals (and noise in the channel, as in [29]). Yet, they rely on the availability of a mesh network for reliable, interference-free communications, and do not account for the impact of fading.

Recently, there has been significant interest in the design of schemes that leverage the waveform superposition properties of wireless channels via OTA computation [30], [31]. Most of these works are based on a centralized FL architecture with a base station acting as PS [4], [11]–[17], [21]. Yet, they rely on assumptions not easily applicable to decentralized settings:

- **CSI:** The works [4], [11]–[15] rely on accurate CSI at transmitters to enable channel inversion and ensure coherent alignment and consistent scaling of the signals received at the PS. However, this approach may not be viable in decentralized settings, where transmitted signals are broadcast to all other devices, each receiving the signals through a different channel; channel estimation

may also be more problematic due to pilot contamination when the number of devices is large [10].

- **Scheduling:** Centralized FL schemes typically require careful power control and device scheduling algorithms to enforce power constraints and ensure device participation. The resulting signaling (typically assumed error-free) may not scale well to decentralized networks.
- **Massive-MIMO:** The work [16] overcomes the need for CSI at the transmitters by assuming a large number of antennas at the PS. Using maximal-ratio combining beamforming at the PS, the destructive effects of interference and noise are mitigated by leveraging the channel hardening effect. However, edge devices with compact form factor may not have large number of antennas.
- **Noise-free downlink:** All these papers (except [13]) assume noise-free downlink. While reasonable for a PS with a typically larger power budget, this assumption may not hold under stringent power constraints of edge devices.

In contrast, the proposed NCOTA-DSGD does not require CSI (at neither transmitters nor receiver) and does not rely on large number of antennas. This is achieved by mapping signals to a set of orthogonal preamble sequences, and by using non-coherent combining at the receivers. NCOTA-DSGD does not rely on power control or scheduling of devices, and is thus scalable to decentralized settings constituted of massive number of devices. Assuming that all communications are subject to noise, fading and interference from concurrent transmissions, NCOTA-DSGD mitigates error propagation via suitable consensus and learning stepsizes.

The preamble-based technique developed in this paper is inspired by [21] developed for *centralized FL* with noise-free downlink channels. Therein, gradient signals are encoded using random vector quantization [32] (i.e., they are mapped randomly to a single codeword) and transmitted via preamble-based random access. In this paper, we do not employ random access nor random vector quantization: instead, we represent a signal as a convex combination of codewords, then mapped to a mixture of orthogonal preamble sequences via a deterministic encoding rule. The scheme developed therein relies on inversion of the average pathloss at the transmitters to ensure an unbiased estimate of the global gradient at the PS (which may violate power constraints under severe pathloss), and on large number of antennas at the PS to achieve vanishing optimality error. In contrast, NCOTA-DSGD achieves vanishing errors without relying on these assumptions.

Some recent works have developed algorithms for decentralized FL that are robust to wireless propagation impairments [18]–[20]. These algorithms mitigate interference by decomposing the network into smaller non-interfering subgraphs, via graph coloring techniques. In each subgraph, one device operates as the PS, which enables the use of techniques described earlier for centralized FL architectures, coupled with a suitable consensus enforcing step similar to (1). However, these schemes may incur severe overhead to enable the acquisition of CSI at the transmitters, power control, and scheduling operations including graph coloring, and may thus not be scalable to massive number of devices. In addition, these papers rely on prior knowledge of the mixing weights ω , used

to enforce consensus in (1). While ω may be estimated via techniques developed in [33], these schemes rely on noise and interference-free links, and may further delay convergence. In this paper, we leverage the structure of the average pathloss as mixing weight, without its explicit knowledge required. While the convergence analysis of [18], [19] reveals a non-vanishing optimality gap, NCOTA-DSGD exhibits vanishing errors, with suitable consensus and learning stepsizes.

Finally, a set of works [34]–[37] proposed a *semi-decentralized* FL architecture, where edge devices collaborate with other neighboring devices unable to form a reliable direct link with the PS. However, these works have similar challenges outlined earlier for centralized and decentralized FL.

B. Summary of contributions and paper organization

In a nutshell, the contributions of this paper are as follows:

- We develop NCOTA-DSGD, a communication-efficient decentralized optimization protocol operating over wireless channels under half-duplex constraints, without CSI nor knowledge of the mixing weights, typically assumed in prior state-of-the-art. We develop a suitable aggregation rule to combine the received signals.
- We analyze the convergence of NCOTA-DSGD, under the assumption of smooth and strongly-convex functions (commonly assumed in the literature, see, e.g., [18], [19]). We demonstrate that, with a suitable choice of decreasing consensus and learning stepsizes, the error (Euclidean distance) between the local optimization variables and the global optimum solution of (P) vanishes with a rate of $\mathcal{O}(k^{-1/4})$ with the number of iterations k .
- We validate numerically the performance of NCOTA-DSGD on an image classification task based on the MNIST dataset [38], casting it as a regularized cross-entropy loss minimization. We demonstrate numerically the superior performance of NCOTA-DSGD when the number of edge devices is large, under stringent delay constraints, with respect to orthogonal digital and analog implementations of DSGD (1).

The rest of this paper is organized as follows. In Sec. II, we present the system model and describe NCOTA-DSGD. In Sec. III, we provide its convergence analysis (proofs provided in the Appendix) under both constant and decreasing stepsizes. In Sec. IV, we present numerical results, followed by concluding remarks in Sec. V.

C. Notation

For a set $\mathcal{S} \subset \mathbb{R}^d$, we denote its interior as $\text{int}(\mathcal{S})$, its boundary as $\text{bd}(\mathcal{S})$, and its convex hull as $\text{conv}(\mathcal{S})$. Unless otherwise stated, all vectors are column. $[\mathbf{a}]_i$ denotes the i th component of vector \mathbf{a} , and $\|\mathbf{a}\| = \sqrt{\mathbf{a}^H \mathbf{a}}$ its Euclidean norm. For a random vector \mathbf{a} , we define $\|\mathbf{a}\|_{\mathbb{E}} \triangleq \sqrt{\mathbb{E}[\|\mathbf{a}\|^2]}$, which coincides with $\|\mathbf{a}\|$ when \mathbf{a} is deterministic; note that $\|\cdot\|_{\mathbb{E}}$ satisfies the triangle inequality $\|\mathbf{a} + \mathbf{b}\|_{\mathbb{E}} \leq \|\mathbf{a}\|_{\mathbb{E}} + \|\mathbf{b}\|_{\mathbb{E}}$ for jointly random vectors \mathbf{a}, \mathbf{b} (a direct consequence of Cauchy-Schwarz and Holder's inequalities). \mathbf{e}_d^m is the m th d -dimensional standard basis vector with $[\mathbf{e}_d^m]_m = 1$, $[\mathbf{e}_d^m]_j = 0, \forall j \neq m$. $\mathbf{1}_d$ and $\mathbf{0}_d$ are the d -dimensional vectors of all ones and all zeros, respectively. \mathbf{I}_d is the $d \times d$ identity matrix. For matrix

\mathbf{A} , $[\mathbf{A}]_{i,j}$ denotes its (i,j) th component, \mathbf{A}^T its transpose, \mathbf{A}^H its complex conjugate transpose. $\mathbb{1}[A]$ is the indicator of event A . Finally, we use the standard big- \mathcal{O} , Θ notations: $\{1\}$ $g(k) = \mathcal{O}(h(k))$ if and only if $\limsup_{k \rightarrow \infty} |g(k)/h(k)| < \infty$; $\{2\}$ $g(k) = \Theta(h(k))$ if and only if $\limsup_{k \rightarrow \infty} |g(k)/h(k)| < \infty$ and $\limsup_{k \rightarrow \infty} |h(k)/g(k)| < \infty$.

II. SYSTEM MODEL AND NCOTA-DSGD

Consider N decentralized nodes solving (P) over wireless channels. We divide time into frames of duration T . Let $\mathbf{w}_{i,k}$ be the local optimization variable of node i , at the start of frame (iteration) k . Then, it generates the signal $\mathbf{x}_{i,k}$ using the *encoding procedure* of Sec. II-A, and transmits it over the wireless channel. It then aggregates the signals received during the frame, via *non-coherent combining* (Secs. II-B and II-C); finally, it updates its \mathbf{w} by combining the aggregate received signal with local stochastic gradient descent (Sec. II-D). Due to randomness of noise, fading, and stochastic gradients, such procedure induces a stochastic process defined on a proper probability space; we denote by \mathcal{F}_k the σ -algebra generated by the signals up to frame k excluded, along with $\mathbf{w}_{i,k}$.

We assume that it is known that the optimizer of (P) lies in a closed, convex and bounded set \mathcal{W} , within which the optimization is restricted. Thus, $\mathbf{w}^* \in \mathcal{W}$ and, initially, $\mathbf{w}_{i,0} \in \mathcal{W}, \forall i$. In the case of strongly-convex global loss function $F(\cdot)$ with strong-convexity parameter μ , as assumed in the convergence analysis of Sec. III (see Assumption 1), \mathcal{W} may be estimated via the global gradient at a reference point, say $\nabla F(\mathbf{0}_d)$. In fact, from strong convexity and the optimality condition $\nabla F(\mathbf{w}^*) = \mathbf{0}_d$, it follows that $\|\nabla F(\mathbf{0}_d)\| = \|\nabla F(\mathbf{0}_d) - \nabla F(\mathbf{w}^*)\| \geq \mu \|\mathbf{0}_d - \mathbf{w}^*\|$. It is then sufficient to restrict (P) to points \mathbf{w} satisfying such inequality, yielding \mathcal{W} as the d -dimensional sphere centered at $\mathbf{0}_d$ with radius $\frac{1}{\mu} \|\nabla F(\mathbf{0}_d)\|$. The global gradient $\nabla F(\mathbf{0}_d) = \frac{1}{N} \sum_{i=1}^N \nabla f_i(\mathbf{0}_d)$ may be estimated by preceding the optimization procedure by an initial consensus phase over the local gradients $\nabla f_i(\mathbf{0}_d)$.

A. Preamble-based Encoding

Let $\mathcal{Z} = \{\mathbf{z}_m \in \mathbb{R}^d : m = 1, \dots, M\}$ be a codebook of M codewords such that $\text{conv}(\mathcal{Z}) \supseteq \mathcal{W}$ (see Example 1), organized into the $d \times M$ matrix $\mathbf{Z} = \sum_m \mathbf{z}_m (\mathbf{e}_M^m)^T$. Therefore, any $\mathbf{w} \in \mathcal{W}$ may be represented as a convex combination of \mathcal{Z} . Let \mathbf{p} denote such convex combination, i.e., $\mathbf{1}_M^T \mathbf{p} = 1$, $[\mathbf{p}]_m \geq 0, \forall m$ and $\mathbf{w} = \sum_{m=1}^M [\mathbf{p}]_m \mathbf{z}_m = \mathbf{Z} \cdot \mathbf{p}$.

Example 1. Let $\mathcal{W} = [-r, r]^d$ (d -dimensional cube). Consider $M = d+1$ codewords $\mathbf{z}_m = 2r d \mathbf{e}_d^m - r \mathbf{1}_d, m = 1, \dots, d$ and $\mathbf{z}_{d+1} = -r \mathbf{1}_d$. For $\mathbf{w} \in \mathcal{W}$, define the $(d+1)$ -dimensional vector

$$[\mathbf{p}]_m = \frac{1}{2rd} (\mathbf{e}_d^m)^T \mathbf{w} + \frac{1}{2d}, \forall m = 1, \dots, d, [\mathbf{p}]_{d+1} = 1 - \sum_{i=1}^d [\mathbf{p}]_i.$$

It is straightforward to see that $[\mathbf{p}]_m \geq 0, \forall m$ and $\mathbf{Z} \cdot \mathbf{p} = \mathbf{w}$, so that \mathbf{p} defines the desired convex combination. The same holds (with the same definition of \mathbf{p}) for a d -dimensional sphere of radius r , $\mathcal{W} \equiv \{\mathbf{w} : \|\mathbf{w}\| \leq r\}$, since it is contained in $[-r, r]^d$.

Example 1 shows that points in a d -dimensional cube or sphere are convex combinations of suitable $(d+1)$ -dimensional codewords, scaling linearly with the problem dimension.

Given $\mathbf{w}_{i,k}$ and the convex combination $\mathbf{p}_{i,k}$ such that $\mathbf{w}_{i,k} = \mathbf{Z} \cdot \mathbf{p}_{i,k}$, node i then generates

$$\mathbf{x}_{i,k} = \sqrt{E} \sum_{m=1}^M \sqrt{[\mathbf{p}_{i,k}]_m} \mathbf{u}_m,$$

where: $\mathcal{U} = \{\mathbf{u}_m \in \mathbb{C}^Q : m = 1, \dots, M\}$ is a set of M orthogonal preambles, each of length $Q \geq M$, with $\|\mathbf{u}_m\| = \sqrt{Q}$; E is the average energy (per sample). In fact, the orthogonality of the preamble sequence and $\mathbf{1}_M^\top \mathbf{p}_{i,k} = 1$ imply that $\frac{1}{Q} \|\mathbf{x}_i(k)\|^2 = E$.

Example 2. One may simply choose $Q = M$ preamble sequences with $\mathbf{u}_m = \sqrt{M} \mathbf{e}_M^n, \forall m$.

B. Transmission over the wireless channel

Each node is then ready to transmit its signal $\mathbf{x}_{i,k}$ over the wireless channel. Assuming half-duplex constraints, we further divide each frame into $S \geq 2$ slots; each node is assigned to transmit in only one of the S slots. This assignment may be performed independently by each node, by choosing one of the S slots uniformly at random, and is kept fixed during the entire optimization session. When N is large, with high probability, each of the S slots has a non-empty set of transmitting nodes. A node transmitting in slot t is in receive mode in all the other slots of frame k . Let $\mathcal{T}(t)$ the set of nodes that transmit in slot $t = 1, \dots, S$, and τ_i be the slot index used by node i for its own transmissions.

Let $h_{i,j}^{k,t} \sim \mathcal{CN}(0, \Lambda_{i,j})$ be the fading channel between transmitting node j and receiving node i in slot t of frame k , i.i.d. over time (both k and t), and independent across links $i - j$. The average pathloss $\Lambda_{i,j}$ depends on factors such as large-scale fading conditions, distance, operating frequency, etc. We assume that $\Lambda_{i,j} = \Lambda_{j,i}$ (channel reciprocity), and that the optimization is carried out over a time interval shorter than fluctuations of large-scale propagation conditions, so that $\Lambda_{i,j}$ does not change over time. This is a scenario characterized, for instance, by stringent delay constraints of the ML application.

In slot t , the nodes $i \notin \mathcal{T}(t)$ receive the signal from the transmitting nodes in $\mathcal{T}(t)$ as $\mathbf{y}_i^{k,t} = \sum_{j \in \mathcal{T}(t)} h_{i,j}^{k,t} \mathbf{x}_{j,k} + \mathbf{n}_i^{k,t}$, where $\mathbf{n}_i^{k,t} \sim \mathcal{CN}(\mathbf{0}_Q, \sigma^2 \mathbf{I}_Q)$ is AWGN noise. The received signal is then correlated with the preamble sequences as

$$\begin{aligned} r_{i,m}^{k,t} &= \frac{\mathbf{u}_m^H \mathbf{y}_i^{k,t}}{\sqrt{E \|\mathbf{u}_m\|^2}} = \sum_{j \in \mathcal{T}(t)} h_{i,j}^{k,t} \frac{\mathbf{u}_m^H \mathbf{x}_{j,k}}{\sqrt{E \|\mathbf{u}_m\|^2}} + \frac{\mathbf{u}_m^H \mathbf{n}_i^{k,t}}{\sqrt{E \|\mathbf{u}_m\|^2}} \\ &= \sum_{j \in \mathcal{T}(t)} h_{i,j}^{k,t} \sqrt{[\mathbf{p}_{j,k}]_m} + n_{i,m}^{k,t}, \quad \forall m = 1, \dots, M, \end{aligned} \quad (2)$$

where $n_{i,m}^{k,t} \triangleq \mathbf{u}_m^H \mathbf{n}_i^{k,t} \sim \mathcal{CN}(0, \sigma^2 / (E \cdot Q))$ is the equivalent noise, i.i.d. over i, k, t, m . Note that,

$$\mathbb{E}[|r_{i,m}^{k,t}|^2 | \mathcal{F}_k] = \sum_{j \in \mathcal{T}(t)} \Lambda_{i,j} [\mathbf{p}_{j,k}]_m + \frac{\sigma^2}{E \cdot Q}, \quad (3)$$

so that $|r_{i,m}^{k,t}|^2$ contains *aggregate* but *noisy* information on the coefficients $[\mathbf{p}_{j,k}]_m$ assigned by nodes $j \in \mathcal{T}(t)$ to codeword \mathbf{z}_m . In the next section, we show that, when properly combined together, these signals approximate the consensus step of (1).

C. Non-Coherent Over-the-Air Consensus

At the end of the frame, each node computes

$$\mathbf{c}_{i,k} = \sum_{t \neq \tau_i} \sum_{m=1}^M \left(|r_{i,m}^{k,t}|^2 - \frac{\sigma^2}{E \cdot Q} \right) (\mathbf{z}_m - \mathbf{w}_{i,k}). \quad (4)$$

Note that $\mathbb{E}[\mathbf{c}_{i,k} | \mathcal{F}_k] = \sum_{j \notin \mathcal{T}(\tau_i)} \Lambda_{i,j} \sum_{m=1}^M (\mathbf{z}_m - \mathbf{w}_{i,k}) [\mathbf{p}_{j,k}]_m$. Since $\sum_{m=1}^M \mathbf{z}_m [\mathbf{p}_{j,k}]_m = \mathbf{w}_{j,k}$, letting $\mathcal{N}_i \triangleq \{1, \dots, N\} \setminus \mathcal{T}(\tau_i)$ be the set of nodes which node i receives from, it follows

$$\mathbb{E}[\mathbf{c}_{i,k} | \mathcal{F}_k] = \sum_{j \in \mathcal{N}_i} \Lambda_{i,j} (\mathbf{w}_{j,k} - \mathbf{w}_{i,k}), \quad (5)$$

so that $\mathbf{c}_{i,k}$ approximates the consensus step in (1), with mixing weights proportional to Λ .

D. Local optimization state update

During the frame, node i computes an unbiased stochastic gradient $\mathbf{g}_{i,k}$ such that $\mathbb{E}[\mathbf{g}_{i,k} | \mathcal{F}_k] = \nabla f_i(\mathbf{w}_{i,k})$. At the end of the frame, it updates $\mathbf{w}_{i,k}$ by combining $\mathbf{c}_{i,k}$ (consensus) with local SGD, followed by projection onto \mathcal{W} , yielding

$$\mathbf{w}_{i,k+1} = \Pi[\mathbf{w}_{i,k} + \gamma_k \mathbf{c}_{i,k} - \eta_k \mathbf{g}_{i,k}], \quad (6)$$

where $\gamma_k, \eta_k > 0$ are *consensus* and *learning* stepsizes, respectively. As shown in Sec. III, these need to be chosen suitably to mitigate the impact of fading, noise and stochastic gradients on convergence to \mathbf{w}^* solution of (P). $\Pi[\mathbf{a}]$ is a projection operator, defined as

$$\Pi[\mathbf{a}] = \arg \min_{\mathbf{w} \in \mathcal{W}} \|\mathbf{w} - \mathbf{a}\|,$$

and guarantees that the algorithm operates within the set \mathcal{W} containing \mathbf{w}^* , i.e., $\mathbf{w}_{i,k} \in \mathcal{W}, \forall i, \forall k$. The process described in Sec. II-A to Sec. II-D is then repeated in frame $k+1$ with the new local optimization variable $\mathbf{w}_{i,k+1}$, and so on. To gain some intuition on (6), let $\Lambda^* \triangleq \max_i \sum_{j \in \mathcal{N}_i} \Lambda_{i,j}$, $\omega_{i,j} = \frac{\Lambda_{i,j}}{\Lambda^*} \cdot \mathbb{1}[j \in \mathcal{N}_i]$ for $i \neq j$ and $\omega_{i,i} = 1 - \sum_{j \neq i} \omega_{i,j}$. From (5), we then find that

$$\mathbb{E}[\mathbf{w}_{i,k} + \gamma_k \mathbf{c}_{i,k} | \mathcal{F}_k] = (1 - \gamma_k \Lambda^*) \mathbf{w}_{i,k} + \gamma_k \Lambda^* \sum_j \omega_{i,j} \mathbf{w}_{j,k}, \quad (7)$$

hence NCOTA-DSGD represents a noisy version of

$$\mathbf{w}_{i,k+1} = \Pi \left[(1 - \gamma_k \Lambda^*) \mathbf{w}_{i,k} + \gamma_k \Lambda^* \sum_j \omega_{i,j} \mathbf{w}_{j,k} - \eta_k \mathbf{g}_{i,k} \right], \quad (8)$$

obtained by replacing $\mathbf{w}_{i,k} + \gamma_k \mathbf{c}_{i,k}$ with its expectation (7). A few observations are in order:

- 1) The weights ω satisfy $\omega_{i,j} \geq 0, \forall i, j$ and $\omega_{i,j} = \omega_{j,i}$, since $\Lambda_{i,j} = \Lambda_{j,i}$ (channel reciprocity) and $\{j \in \mathcal{N}_i\} \Leftrightarrow \{i \in \mathcal{N}_j\}$. Hence, $[\Omega]_{i,j} = \omega_{i,j}$ is a symmetric, doubly-stochastic mixing matrix induced by the large-scale propagation conditions of the channel.
- 2) By specializing the noise-free dynamics (8) to $\gamma_k = (\Lambda^*)^{-1}, \forall k$ and neglecting the projection operation, they reduce to the DSGD updates in (1). Therefore, NCOTA-DSGD can be interpreted as a projected DSGD with noisy consensus. The consensus stepsize γ_k helps mitigate the detrimental effect of error propagation due to noise and

fading in the channel. Remarkably, unlike (1), no explicit knowledge of ω is required in NCOTA-DSGD.

- 3) The noise-free dynamics (8) follow the *adapt-then-combine* implementation of DGD (see also [39, Chapter 7]), i.e., local gradients are based on $\mathbf{w}_{i,k}$ available at the beginning of the frame. This allows nodes to compute gradients in parallel with data transmission and reception during the frame duration. Such parallel processing would not be possible with the *combine-then-adapt* implementation [39, Chapter 7], in which gradients are based on $\sum_j \omega_{i,j} \mathbf{w}_{j,k}$ available only at the end of the frame, after all signals have been received.

Letting W_{tot} be the communication bandwidth, the frame duration of NCOTA-DSGD is

$$T = \frac{S \cdot Q}{W_{tot}}. \quad (9)$$

In fact, each frame includes S slots, and in each slot a signal of Q samples is transmitted. Based on the Examples 1 and 2, and assuming the nodes are partitioned into $S = 2$ sets, we find $Q = M = d + 1$, yielding $T = \frac{2(d+1)}{W_{tot}}$, which depicts a linearly-increasing frame duration with the problem dimension d . The use of compression techniques to improve scalability (see, e.g., [18]) is left for future work.

III. CONVERGENCE ANALYSIS

We first rewrite NCOTA-DSGD more compactly, and isolate the error terms (Sec. III-A). We then introduce the assumptions and definitions used in the analysis (Sec. III-B). We present the main convergence result in Sec. III-C, specialized to the cases of constant (Sec. III-D) and decreasing (Sec. III-E) stepsizes. A discussion follows in Sec. III-F.

A. Equivalent representation of NCOTA-DSGD updates

We use lower-case variables to denote the signals of a certain node (\mathbf{a}_i for the \mathbf{a} -signal of node i), and upper-case variables to denote the local signals stacked over the network ($\mathbf{A} = \sum_{i=1}^N \mathbf{e}_N^i \otimes \mathbf{a}_i$). Hence, \mathbf{W}_k , \mathbf{G}_k , \mathbf{C}_k stack the $\mathbf{w}_{i,k}$, $\mathbf{g}_{i,k}$, $\mathbf{c}_{i,k}$ -signals over the network. Let

$$f(\mathbf{W}) = \sum_{i=1}^N f_i(\mathbf{w}_i). \quad (10)$$

We then stack the updates (6) as $\mathbf{W}_{k+1} = \Pi^N[\mathbf{W}_k + \gamma_k \mathbf{C}_k - \eta_k \mathbf{G}_k]$, where $\mathbb{E}[\mathbf{G}_k | \mathcal{F}_k] = \nabla f(\mathbf{W}_k)$ and $\Pi^N[\cdot]$ projects its argument onto \mathcal{W}^N . Further simplification is obtained by isolating the errors due to fading and noise ($\epsilon_k^{(1)}$), and due to stochastic gradients ($\epsilon_k^{(2)}$). These are defined as

$$\epsilon_k^{(1)} = \mathbf{C}_k - \mathbb{E}[\mathbf{C}_k | \mathcal{F}_k], \quad \epsilon_k^{(2)} = \mathbf{G}_k - \nabla f(\mathbf{W}_k),$$

respectively. It is straightforward to see that $\mathbb{E}[\epsilon_k^{(1)} | \mathcal{F}_k] = \mathbb{E}[\epsilon_k^{(2)} | \mathcal{F}_k] = \mathbf{0}_{Nd}$. Letting $\hat{\Omega} = \Omega \otimes \mathbf{I}_d$, we then rewrite

$$\mathbf{W}_{k+1} = \Pi^N \left[\underbrace{(1 - \gamma_k \Lambda^*) \mathbf{W}_k + \gamma_k \Lambda^* \hat{\Omega} \mathbf{W}_k - \eta_k \nabla f(\mathbf{W}_k)}_{(a)} + \underbrace{\gamma_k \epsilon_k^{(1)} - \eta_k \epsilon_k^{(2)}}_{(b)} \right]. \quad (11)$$

The term (a) specializes to the standard DGD update (1) when $\gamma_k = (\Lambda^*)^{-1}$; (b) (referred to as the "noise" in the remainder), instead, captures the effect of AWGN noise, channel fading, and stochastic gradients. Following an approach similar to [8] for the analysis of DGD (therein, with *fixed* stepsize), we interpret the term (a) as a centralized gradient descent update with stepsize η_k , based on the Lyapunov function

$$G_k(\mathbf{W}) \triangleq f(\mathbf{W}) + \frac{\gamma_k \Lambda^*}{2\eta_k} \mathbf{W}^\top (\mathbf{I}_{Nd} - \hat{\Omega}) \mathbf{W},$$

where the second term enforces consensus among the nodes in the network (in fact, it equals zero when $\mathbf{w}_i = \mathbf{w}_j, \forall i, j$). Note that G_k is time-varying due to k -dependent stepsizes, thus generalizing [8] based on a fixed stepsize. We can then express (11) compactly as

$$\mathbf{W}_{k+1} = \Pi^N[\mathbf{W}_k - \eta_k \nabla G_k(\mathbf{W}_k) + \gamma_k \epsilon_k^{(1)} - \eta_k \epsilon_k^{(2)}]. \quad (12)$$

B. Assumptions and definitions

We study the convergence of NCOTA-DSGD under the following standard assumptions.

Assumption 1. All $f_i(\mathbf{w})$ are μ -strongly convex, L -smooth.

A direct consequence of Assumption 1 is that the global F in (P) and f in (10) are also μ -strongly convex and L -smooth.

Assumption 2. $\mathbf{w}^* \in \text{int}(\mathcal{W})$, hence its distance from the boundary of \mathcal{W} satisfies $\zeta \triangleq \min_{\mathbf{w} \in \text{bd}(\mathcal{W})} \|\mathbf{w} - \mathbf{w}^*\| > 0$.

While our analysis may be relaxed when \mathbf{w}^* lies on the boundary of \mathcal{W} ($\zeta = 0$), it generally leads to looser convergence results. As discussed after (8), Ω is symmetric and doubly-stochastic, hence all its eigenvalues (ρ_i for the i th one) are real and such that $1 = \rho_1 \geq \rho_2 \geq \dots \geq \rho_N \geq -1$. We make the following standard assumption on ρ_2 .

Assumption 3. $\rho_2 < 1$.

Finally, we make the following assumption on $\epsilon_k^{(1)}$ and $\epsilon_k^{(2)}$.

Assumption 4. There exist $\Sigma^{(1)}, \Sigma^{(2)} \geq 0$ such that

$$\frac{1}{N} \mathbb{E}[\|\epsilon_k^{(1)}\|^2 | \mathcal{F}_k] \leq \Sigma^{(1)}, \quad \frac{1}{N} \mathbb{E}[\|\epsilon_k^{(2)}\|^2 | \mathcal{F}_k] \leq \Sigma^{(2)}.$$

Appendix A provides closed-form expressions under Rayleigh fading and minibatch gradients.

The following definition follows since \mathcal{W} is bounded.

Definition 1 (diameter of \mathcal{W}). $d_{\mathcal{W}} \triangleq \max_{\mathbf{w}_1, \mathbf{w}_2 \in \mathcal{W}} \|\mathbf{w}_1 - \mathbf{w}_2\|$.

Lastly, we define the following gradient bound.

Definition 2 (gradient bound at \mathbf{w}^*). $\|\nabla f_i(\mathbf{w}^*)\| \leq \nabla_{\max}, \forall i$.

Note that ∇_{\max} may be simply chosen as $\triangleq \max_i \|\nabla f_i(\mathbf{w}^*)\|$.

C. Main convergence results

We are now ready to present the convergence properties of NCOTA-DSGD. The main idea is to decompose the error $\|\mathbf{W}_k - \mathbf{1} \otimes \mathbf{w}^*\|$ between the local optimization variables and the global optimum into: {1} the error between \mathbf{W}_k and the noise-free dynamics $\tilde{\mathbf{W}}_k$ obtained under no noise (see (13));

{2} the error between $\tilde{\mathbf{W}}_k$ and the minimizer of the Lyapunov function G_k (see (14)); and {3} the error between the latter and the global optimum \mathbf{w}^* . We restrict our analysis to $k \geq \bar{k}$ under a suitably chosen \bar{k} (to be defined later), representing a regime in which stepsizes become sufficiently small to satisfy certain conditions stated in Theorem 1.¹ Accordingly, let $\tilde{\mathbf{W}}_k$ be the noise-free dynamics, initialized as $\tilde{\mathbf{W}}_{\bar{k}} = \mathbf{W}_{\bar{k}}$ and

$$\tilde{\mathbf{W}}_{k+1} = \Pi^N[\tilde{\mathbf{W}}_k - \eta_k \nabla G_k(\tilde{\mathbf{W}}_k)], \quad \forall k \geq \bar{k}, \quad (13)$$

obtained by setting the noise in (11) as $\mathbf{0}_{Nd}$. Furthermore, define the minimizer of G_k as

$$\mathbf{W}_k^* = \arg \min_{\mathbf{W} \in \mathcal{W}^N} G_k(\mathbf{W}). \quad (14)$$

With these definitions, we bound the error between the local $\mathbf{w}_{i,k}$ and global optimum \mathbf{w}^* as

$$\begin{aligned} \sqrt{\mathbb{E} \left[\frac{1}{N} \sum_i \|\mathbf{w}_{i,k} - \mathbf{w}^*\|^2 \right]} &= \frac{1}{\sqrt{N}} \|\mathbf{W}_k - \mathbf{1}_N \otimes \mathbf{w}^*\|_{\mathbb{E}} \\ &= \frac{1}{\sqrt{N}} \|(\mathbf{W}_k - \tilde{\mathbf{W}}_k) + (\tilde{\mathbf{W}}_k - \mathbf{W}_k^*) + (\mathbf{W}_k^* - \mathbf{1}_N \otimes \mathbf{w}^*)\|_{\mathbb{E}} \\ &\leq \frac{1}{\sqrt{N}} \|\mathbf{W}_k - \tilde{\mathbf{W}}_k\|_{\mathbb{E}} + \frac{1}{\sqrt{N}} \|\tilde{\mathbf{W}}_k - \mathbf{W}_k^*\|_{\mathbb{E}} \\ &\quad + \frac{1}{\sqrt{N}} \|\mathbf{W}_k^* - \mathbf{1}_N \otimes \mathbf{w}^*\|, \end{aligned} \quad (15)$$

where the last step follows from the triangle inequality. These terms are individually bounded in Theorem 1. To this end, let

$$P_{\ell,k} \triangleq \prod_{j=\ell}^{k-1} (1 - \mu \eta_j), \quad k \geq \ell \geq \bar{k}. \quad (16)$$

Theorem 1. Assume $\forall k \geq \bar{k}$: $\eta_k(\mu + L) + \gamma_k \Lambda^*(1 - \rho_N) \leq 2$ (C1); $\frac{\eta_k}{\gamma_k} \leq \frac{\zeta \cdot Z}{\sqrt{N} \Delta_{\max}}$ (C2), where $Z \triangleq \frac{(1 - \rho_2) \Lambda^*}{2\sqrt{1 + L/\mu}}$; $\frac{\gamma_k}{\eta_k} \leq \frac{\gamma_{k+1}}{\eta_{k+1}}$ (C3). Then,

$$\frac{1}{\sqrt{N}} \|\mathbf{W}_k - \tilde{\mathbf{W}}_k\|_{\mathbb{E}} \leq \left[\sum_{\ell=\bar{k}}^{k-1} P_{\ell+1,k}^2 \left(\gamma_{\ell}^2 \Sigma^{(1)} + \eta_{\ell}^2 \Sigma^{(2)} \right) \right]^{\frac{1}{2}}, \quad (17)$$

$$\begin{aligned} \frac{1}{\sqrt{N}} \|\tilde{\mathbf{W}}_k - \mathbf{W}_k^*\|_{\mathbb{E}} &\leq d_{\mathcal{W}} P_{\bar{k},k} \\ &\quad + \frac{\nabla_{\max} + L d_{\mathcal{W}}}{Z} \sum_{\ell=\bar{k}}^{k-1} P_{\ell+1,k} \left(\frac{\gamma_{\ell+1}}{\eta_{\ell+1}} - \frac{\gamma_{\ell}}{\eta_{\ell}} \right) \frac{\eta_{\ell}^2}{\gamma_{\ell}^2}, \end{aligned} \quad (18)$$

$$\frac{1}{\sqrt{N}} \|\mathbf{W}_k^* - \mathbf{1}_N \otimes \mathbf{w}^*\| \leq \frac{\Delta_{\max}}{Z} \frac{\eta_k}{\gamma_k}. \quad (19)$$

Proof. See Appendix B. \square

The first term (17), bounding the error between the noisy and noise-free dynamics, shows the impact of the noise variances $\Sigma^{(1)}$ and $\Sigma^{(2)}$. The second term (18), bounding the error between the noise-free dynamics and the minimizer of the Lyapunov function G_k , is composed of two terms: the first ($d_{\mathcal{W}} P_{\bar{k},k}$) accounts for the initial error at time \bar{k} ; the second term is a direct result of time-varying stepsizes (in fact, it is zero when η_k and γ_k are constant), and follows from the need to track the minimizer \mathbf{W}_k^* of G_k , as k varies. The last term (19) shows that the minimizer \mathbf{W}_k^* of G_k approximates

¹For $k < \bar{k}$, one can trivially bound $\|\mathbf{w}_{i,k} - \mathbf{w}^*\| \leq d_{\mathcal{W}}$, since $\mathbf{w}_{i,k} \in \mathcal{W}$.

\mathbf{w}^* arbitrarily well, by choosing η_k/γ_k sufficiently small. We now specialize Theorem 1 to the case of constant stepsizes (Sec. III-D). This study will provide insights on the design of decreasing stepsizes in Sec. III-E.

D. Constant stepsizes

Let $\eta_k = \eta > 0$, $\gamma_k = \gamma > 0, \forall k$. To satisfy C1-C3 of Theorem 1, we further require: $\eta(\mu + L) + \gamma \Lambda^*(1 - \rho_N) \leq 2$ and $\frac{\eta}{\gamma} \leq \frac{\zeta \cdot Z}{\sqrt{N} \nabla_{\max}}$ with $\bar{k} = 0$. Then, (16) specializes as $P_{\ell,k} = (1 - \mu \eta)^{k-\ell}$, and (17)-(19) as²

$$\frac{1}{\sqrt{N}} \|\mathbf{W}_k - \tilde{\mathbf{W}}_k\|_{\mathbb{E}} \leq \sqrt{\Sigma^{(1)} + \eta^2 \gamma^{-2} \Sigma^{(2)}} \frac{\gamma}{\sqrt{\mu \eta}}, \quad (20)$$

$$\frac{1}{\sqrt{N}} \|\tilde{\mathbf{W}}_k - \mathbf{W}_k^*\|_{\mathbb{E}} \leq d_{\mathcal{W}} P_{0,k} \leq d_{\mathcal{W}} e^{-\mu \eta k}, \quad (21)$$

$$\frac{1}{\sqrt{N}} \|\mathbf{W}_k^* - \mathbf{1}_N \otimes \mathbf{w}^*\| \leq \frac{\Delta_{\max}}{Z} \frac{\eta}{\gamma}. \quad (22)$$

To make these errors small, $\gamma/\sqrt{\eta}$, η/γ and $e^{-\mu \eta k}$ need all be small, yielding a trade-off between the two stepsizes. To further investigate the convergence properties, let us consider a target timeframe K when the algorithm stops. It appears then reasonable to choose $\eta = a \cdot K^{-x}$ and $\gamma = b \cdot K^{-y}$ for suitable $a, b, x, y > 0$. Under this choice, $e^{-\mu \eta K}$ requires $x < 1$ to converge when $K \rightarrow \infty$, whereas (20) and (22) become

$$\frac{1}{\sqrt{N}} \|\mathbf{W}_K - \tilde{\mathbf{W}}_K\|_{\mathbb{E}} \leq \frac{b}{\sqrt{a \mu}} \sqrt{\Sigma^{(1)} + (a/b)^2 \Sigma^{(2)} K^{2(y-x)} K^{\frac{x}{2}-y}},$$

$$\frac{1}{\sqrt{N}} \|\mathbf{W}_K^* - \mathbf{1}_N \otimes \mathbf{w}^*\| \leq \frac{\Delta_{\max}}{Z} \frac{a}{b} K^{y-x},$$

i.e., they decay as $K^{\max\{y-x, x/2-y\}}$ in the worst case. Minimizing $\max\{y-x, x/2-y\}$ under $x < 1$ yields $y = 3/4(1-\epsilon)$, $x = 1-\epsilon$ for any small $\epsilon > 0$. With this choice, (21) becomes

$$\frac{1}{\sqrt{N}} \|\tilde{\mathbf{W}}_k - \mathbf{W}_k^*\|_{\mathbb{E}} \leq d_{\mathcal{W}} e^{-\mu a \cdot K^{\epsilon}} \leq d_{\mathcal{W}} \left[\frac{1-\epsilon}{4 \mu a \epsilon} \right]^{\frac{1-\epsilon}{4 \epsilon}} K^{-\frac{1-\epsilon}{4}}, \quad (23)$$

so that all error terms (hence the overall error) scale as $\mathcal{O}(K^{-1/4(1-\epsilon)})$ for a target timeframe K . A similar convergence rate is shown in [40] under a different setup but similar tuning of the consensus and learning stepsizes given K :³ it assumes quantization, error-free communications, constant stepsizes. This analysis unveils some drawbacks of using constant stepsizes: {1} faster convergence rate is achieved with smaller ϵ (approaching $\mathcal{O}(K^{-1/4})$), at the cost of larger scaling coefficients in (23); {2} tuning of η and γ requires prior knowledge of the target timeframe K , as well as of Λ^* , ρ_2 , ρ_N , ζ , ∇_{\max} to satisfy C1-C2 of Theorem 1. In the next section, we show that these limitations and the dependence on ϵ are overcome via decreasing stepsizes.

E. Decreasing stepsizes

The previous analysis suggests that $\gamma_k = \Theta(k^{-3/4})$ and $\eta_k = \Theta(k^{-1})$ to guarantee convergence. Accordingly, we choose $\gamma_k = \gamma_0 \delta^{3/4} (k + \delta)^{-3/4}$ and $\eta_k = \eta_0 \delta (k + \delta)^{-1}$ with

²Here, we use the fact that $\eta(\mu + L) + \gamma \Lambda^*(1 - \rho_N) \leq 2$ implies $\eta \leq 1/\mu$.

³Note that $\alpha, \epsilon, \delta, T$ used in [40, Theorem 1] map as $\alpha \rightarrow \eta/\gamma$, $\epsilon \rightarrow \gamma$, $\delta \rightarrow (1-\epsilon)/2$, $T \rightarrow K$ in our paper

initial stepsizes $\gamma_0 > 0$, $\eta_0 > 0$, and delay $\delta > 0$ preventing η_k, γ_k from decaying too quickly. Under this choice: $\{1\}$ γ_k/η_k is non-decreasing in k (C3 of Theorem 1); $\{2\}$ since $\eta_k \rightarrow 0$, $\gamma_k \rightarrow 0$ and $\eta_k/\gamma_k \rightarrow 0$ for $k \rightarrow \infty$, there exists $\bar{\kappa} \geq 0$ such that C1-C2 of Theorem 1 are satisfied $\forall k \geq \bar{\kappa}$. The following result specializes Theorem 1 to this choice.

Theorem 2. Let $\gamma_k = \gamma_0 \delta^{3/4} (k + \delta)^{-3/4}$, $\eta_k = \eta_0 \delta (k + \delta)^{-1}$ with $\eta_0 > 0$, $\gamma_0 > 0$ and $\delta \geq \frac{5}{4\mu\eta_0}$. Let $\bar{\kappa} \geq 0$ such that the conditions C1-C2 of Theorem 1 are satisfied. Then, $\forall k \geq \bar{\kappa}$,

$$\frac{1}{\sqrt{N}} \|\mathbf{W}_k - \tilde{\mathbf{W}}_k\|_{\mathbb{E}} \leq \frac{\sqrt{5}e}{2\sqrt{\mu}} \left[\frac{\gamma_0}{\sqrt{\eta_0}} \sqrt{\Sigma^{(1)}} + \sqrt{\eta_0} \sqrt{\Sigma^{(2)}} \delta^{1/4} (k + \delta)^{-1/4} \right] \delta^{1/4} (k + \delta)^{-1/4}, \quad (24)$$

$$\frac{1}{\sqrt{N}} \|\tilde{\mathbf{W}}_k - \mathbf{W}_k^*\|_{\mathbb{E}} \leq d_{\mathcal{W}} \left(1 + \frac{k - \bar{\kappa}}{\bar{\kappa} + \delta} \right)^{-5/4} + \frac{\nabla_{\max} + L d_{\mathcal{W}}}{Z} \frac{e}{4} \frac{\eta_0}{\gamma_0} \delta^{1/4} (k + \delta)^{-1/4}, \quad (25)$$

$$\frac{1}{\sqrt{N}} \|\mathbf{W}_k^* - \mathbf{1}_N \otimes \mathbf{w}^*\| \leq \frac{\nabla_{\max}}{Z} \frac{\eta_0}{\gamma_0} \delta^{1/4} (k + \delta)^{-1/4}. \quad (26)$$

Proof. See Appendix C. \square

F. Discussion

Combining these results into (15), it readily follows that

$$\sqrt{\mathbb{E} \left[\sum_i \|\mathbf{w}_{i,k} - \mathbf{w}^*\|^2 \right]} = \mathcal{O}(k^{-1/4}). \quad (27)$$

To get some intuition behind this result, consider (11) with fixed $\gamma_k = 1/\Lambda^*$ and no projection:

$$\mathbf{W}_{k+1} = \hat{\Omega} \mathbf{W}_k - \eta_k \nabla f(\mathbf{W}_k) + \epsilon_k^{(tot)}, \quad (28)$$

where $\epsilon_k^{(tot)} \triangleq (\Lambda^*)^{-1} \epsilon_k^{(1)} - \eta_k \epsilon_k^{(2)}$ is the overall noise. When $\epsilon_k^{(1)} = \mathbf{0}_{Nd}$, i.e., only stochastic gradients contribute to the noise, one can see that (28) specializes to the DSGD algorithm (1), whose error is known to converge to 0 with rate $\mathcal{O}(k^{-1/2})$, when $\eta_k = \Theta(k^{-1})$ [41]. To obtain this result, $\|\epsilon_k^{(tot)}\|_{\mathbb{E}}$ should be of order $\mathcal{O}(k^{-1})$. This property indeed holds when stochastic gradients are the only noise source, since $\|-\eta_k \epsilon_k^{(2)}\|_{\mathbb{E}} \leq \eta_k \sqrt{N \Sigma^{(2)}}$, but is lost with fading and AWGN noise ($\epsilon_k^{(1)}$), since $\|\epsilon_k^{(tot)}\|_{\mathbb{E}}$ becomes $\mathcal{O}(1)$, requiring stronger noise mitigation via the consensus stepsize γ_k , at the cost of slower convergence ($\mathcal{O}(k^{-1/4})$).

It is also interesting to compare NCOTA-DSGD to a two-timescale algorithm that mitigates noise as follows: instead of updating \mathbf{W} at the end of each frame as in NCOTA-DSGD, it perform these updates only at specific frames $0 = K_0 < K_1 < \dots < K_t$ indexed by $t \geq 0$; between K_t and K_{t+1} , each node transmits a fixed signal $\mathbf{w}_{i,t}$, following the encoding procedure described in Sec. II-A, and computes a sample average of the signals received from K_t to K_{t+1} to mitigate AWGN noise and fading. At K_{t+1} , $\mathbf{W}_{t+1} = \hat{\Omega} \mathbf{W}_t - \eta_t \nabla f(\mathbf{W}_t) + \epsilon_t^{(tot)}$, where $\epsilon_t^{(tot)}$ now accounts for the noise averaged over $K_{t+1} - K_t$ iterations. By choosing $K_t = t^3$ (i.e. $K_{t+1} - K_t \approx 3t^2$) and $\eta_t = \Theta(t^{-1})$, it is straightforward to see that $\|\epsilon_t^{(tot)}\|_{\mathbb{E}} = \mathcal{O}(t^{-1})$, which satisfies the previous property and guarantees a convergence rate of $\mathcal{O}(t^{-1/2})$. However, since these t iterates

require $k = t^3$ timeframes to be completed, this two-timescale scheme converges with rate $\mathcal{O}(k^{-1/6})$ after k timeframes. The faster convergence of NCOTA-DSGD ($\mathcal{O}(k^{-1/4})$) is attributed to an improved noise mitigation through the use of a small consensus stepsize $\gamma_k = \Theta(k^{-3/4})$.

IV. NUMERICAL RESULTS

We consider the MNIST dataset [38], containing 70K images of hand-written digits (0 to 9), to be classified.

Network deployment: We consider a network with N (to be varied) nodes, spread uniformly at random over a circular region, with a density of $\lambda = 14$ nodes/km² (radius $\sqrt{N/(\pi\lambda)}$). The nodes communicate over a bandwidth $W_{tot} = 1$ MHz, carrier frequency $f_c = 3$ GHz. The pathloss between node i and j follows Friis' free space equation with pathloss exponent 2. All nodes transmit with power $P_{tx} = 20$ dBm (energy per sample $E = P_{tx}/W_{tot}$). The noise power spectral density is $N_0 = -173$ dBm/Hz (noise variance $\sigma^2 = N_0$).

Data deployment: We use 1200 data points (120 for each digit). Each node has a local dataset of $1200/N$ images from a single digit, so that $N/10$ nodes have only images of digit '0', $N/10$ nodes of digit '1', and so on. Cooperation is then necessary to solve the classification task, due to lack of examples of other digits at any single node. To speed up the simulation time, each 28×28 pixels image is first cropped down to 100 pixels; the corresponding feature $\mathbf{d} \in \mathbb{R}^{100}$ is then normalized to $\|\mathbf{d}\| = 1$. These features and their corresponding labels $\ell \in \{0, \dots, 9\}$ form the local dataset \mathcal{D}_i of node i .

Optimization problem formulation: We solve the task via a regularized cross-entropy loss, defined for a feature vector $\mathbf{d} \in \mathbb{R}^{100}$ with label $\ell \in \{0, \dots, 9\}$ as

$$\phi(\ell, \mathbf{d}; \mathbf{w}) = \frac{\mu}{2} \|\mathbf{w}\|^2 - \ln \left(\frac{\exp\{\mathbf{d}^\top \mathbf{w}^{(\ell)}\}}{\sum_{j=0}^9 \exp\{\mathbf{d}^\top \mathbf{w}^{(j)}\}} \right),$$

where: $\mathbf{w}^\top = [\mathbf{w}^{(1)\top}, \dots, \mathbf{w}^{(9)\top}] \in \mathbb{R}^d$ is a $d=900$ -dimensional parameter vector, with $\mathbf{w}^{(\ell)} \in \mathbb{R}^{100}$; $\mathbf{w}^{(0)} = \mathbf{0}_{100}$ (since the cross-entropy loss is shift-invariant); $\mu=0.01>0$ scales the ℓ_2 regularization. Accordingly, $f_i(\mathbf{w}) = \frac{1}{|\mathcal{D}_i|} \sum_{(\ell, \mathbf{d}) \in \mathcal{D}_i} \phi(\ell, \mathbf{d}; \mathbf{w})$.

It can be shown that ϕ , the local and global functions f_i , $F = \frac{1}{N} \sum_i f_i$, are all μ -strongly-convex and $L=\mu+2$ -smooth. \mathcal{W} is chosen as the d -dimensional sphere with center $\mathbf{0}_d$ and radius $r = \frac{1}{\mu} \|\nabla F(\mathbf{0}_d)\|$ (see Sec. II).

At each node, gradients are computed using minibatches $\mathcal{B}_{i,k} \subseteq \mathcal{D}_i$. Assuming that each gradient computation $\nabla \phi$ on a single datapoint takes $T_{grad} = 1$ ms, computing the gradient over the minibatch $\mathcal{B}_{i,k}$ takes $|\mathcal{B}_{i,k}| T_{grad}$. These computations are done in parallel with communications, hence the minibatch size $|\mathcal{B}_{i,k}| = \min\{\lfloor T/T_{grad} \rfloor, 1200/N\}$ depends on the frame duration T of each algorithm (see next).

Algorithms: All are initialized as $\mathbf{w}_{i,0} = \mathbf{0}_d, \forall i$.

• **NCOTA-DSGD** (proposed algorithm): To enforce half-duplex constraints, the nodes are partitioned into $S = 2$ sets, each with $N/2$ randomly selected nodes. We use $M = d + 1$ codewords as in Example 1, and $Q = M$ preambles as in Example 2, yielding the frame duration $T \approx 1.8$ ms and minibatches of size $|\mathcal{B}_{i,k}| = 1$. We use stepsizes as in Theorem 2,

with $\eta_0 = (\mu + L)^{-1}$, $\gamma_0 = (40\Lambda^*(1 - \rho_2))^{-1}$, $\delta = \frac{5}{4\mu\eta_0}$, tuned to achieve good overall performance.

In addition, we implement DSGD over orthogonal digital (OD-) and analog (OA-) channels, following the updates

$$\mathbf{w}_{i,k+1} = \Pi[\mathbf{w}_{i,k} + \mathbf{c}_{i,k} - \eta \cdot \mathbf{g}_{i,k}], \quad \mathbb{E}[\mathbf{g}_{i,k}] = \nabla f_i(\mathbf{w}_{i,k}); \quad (29)$$

$\mathbf{c}_{i,k}$ is a reconstruction of the consensus $\sum_j \omega_{i,j}(\mathbf{w}_{j,k} - \mathbf{w}_{i,k})$; η is optimized numerically for fast convergence. OD/OA-DSGD differ in how signals are encoded and $\mathbf{c}_{i,k}$ is computed:

- **OD-DSGD**: each node scales $\mathbf{w}_{i,k}$ by the largest magnitude $\|\mathbf{w}_{i,k}\|_\infty$; each component of $\mathbf{w}_{i,k}/\|\mathbf{w}_{i,k}\|_\infty$ (each $\in [-1, 1]$) is then quantized using 5 quantization levels uniformly spaced in $[-1, 1]$. We use dithered quantization: the quantized vector, $\hat{\mathbf{w}}_{i,k}$, is such that $\mathbb{E}[\hat{\mathbf{w}}_{i,k}] = \mathbf{w}_{i,k}$. With $\|\mathbf{w}_{i,k}\|_\infty$ encoded using machine precision (64 bits), the data payload is thus $L = 64 + d \log_2(5) \approx 2154$ bits, then transmitted by each node over orthogonal channels (via TDMA), using capacity achieving codes with rate $R \approx 9$ [bits/s/Hz], yielding $\leq 10\%$ outage probability for nodes within a 500m radius from the transmitter, and resulting in a frame duration of $T = N \cdot L / R / W_{tot}$. With the fading channel $h_{i,j} \sim \mathcal{CN}(0, \Lambda_{i,j})$ between transmitting node j and receiving node i , and assuming CSI at the receiver, the probability of successful reception of the signal transmitted by node j and received at i is $P_{i,j}^{succ} \triangleq \exp\{-\frac{\sigma^2}{E\Lambda_{i,j}}(2^R - 1)\}$. At the end of the N transmissions, node i computes

$$\mathbf{c}_{i,k} = \sum_{j \neq i} \frac{\iota_{i,j}^k}{\max_{n \in \{i,j\}} \{\sum_{\ell \neq n} P_{n,\ell}^{succ}\}} (\hat{\mathbf{w}}_{j,k} - \mathbf{w}_{i,k}),$$

where $\iota_{i,j}^k = \mathbb{1}[R < \log_2(1 + |h_{i,j}|^2 E / \sigma^2)]$ indicates a successful reception of $\hat{\mathbf{w}}_{j,k}$ at node i . With this choice of $\mathbf{c}_{i,k}$, the updates (29) represent a noisy version of (1) with weights $\omega_{i,j} = \frac{P_{i,j}^{succ}}{\max_{n \in \{i,j\}} \{\sum_{\ell \neq n} P_{n,\ell}^{succ}\}}$, $j \neq i$ and $\omega_{i,i} = 1 - \sum_{j \neq i} \omega_{i,j}$ (seen by taking the expectation of $\mathbf{c}_{i,k}$, with respect to fading and random quantization), and the additional projection.

- **OA-DSGD**: $\mathbf{w}_{i,k}$ is first normalized to unit norm; the first (respectively, second) half of the normalized vector $\frac{[\mathbf{w}_{i,k}]_{1:d/2}}{\|\mathbf{w}_{i,k}\|}$ ($\frac{[\mathbf{w}_{i,k}]_{d/2+1:d}}{\|\mathbf{w}_{i,k}\|}$) is mapped to the real (imaginary) part of the baseband transmitted signal. Two additional samples are used to transmit the norm $\|\mathbf{w}_{i,k}\|$, and a pilot signal to estimate the channel at the receiver. This yields the $(d/2+2)$ -dimensional complex-valued signal

$$\mathbf{x}_{i,k} = \alpha_{i,k} \left[\frac{[\mathbf{w}_{i,k}]_{1:d/2} + j[\mathbf{w}_{i,k}]_{d/2+1:d}}{\|\mathbf{w}_{i,k}\|} ; \frac{1}{r} \|\mathbf{w}_{i,k}\| ; 1 \right],$$

where $\alpha_{i,k}$ is a scaling factor chosen to guarantee the energy constraint $\|\mathbf{x}_{i,k}\|^2 = E(d/2+2)$. The signal is then transmitted by each node over orthogonal channels (via TDMA), yielding the frame duration $T = N \cdot (d/2+2) / W_{tot}$. With the fading channel $h_{i,j} \sim \mathcal{CN}(0, \Lambda_{i,j})$ between transmitting node j and receiving node i , the signal $\mathbf{y}_{i,j} = h_{i,j} \mathbf{x}_{j,k} + \mathbf{n}_{i,j}$ with $\mathbf{n}_{i,j} \sim \mathcal{CN}(\mathbf{0}_{d/2+2}, \sigma^2 \mathbf{I}_{d/2+2})$, received by node i is processed as follows: first, $\alpha_{i,k} h_{i,j}$ is estimated from the last sample via maximum likelihood as $\widehat{\alpha_{i,k} h_{i,j}}$; $\|\mathbf{w}_{i,k}\|$ is then estimated from the penultimate sample as $\widehat{\|\mathbf{w}_{i,k}\|}$; finally, the overall signal is estimated by extracting the real and imaginary

components of the first $d/2$ samples of $\mathbf{y}_{i,j} \widehat{\alpha_{i,k} h_{i,j}} / \widehat{\|\mathbf{w}_{i,k}\|}$, so that the signal $\mathbf{w}_{j,k}$ transmitted by node j is reconstructed as $\hat{\mathbf{w}}_{j,k}$ at node i . After receiving the signals from all nodes, node i then computes

$$\mathbf{c}_{i,k} = \sum_{j \neq i} \frac{\Lambda_{i,j}}{\max_{n \in \{i,j\}} \{\sum_{\ell \neq n} \Lambda_{n,\ell}\}} (\hat{\mathbf{w}}_{j,k} - \mathbf{w}_{i,k}),$$

so that signals are mixed proportionally to the average channel strength. With this choice of $\mathbf{c}_{i,k}$, the updates (29) represent a noisy version of (1) with $\omega_{i,j} = \frac{\Lambda_{i,j}}{\max_{n \in \{i,j\}} \{\sum_{\ell \neq n} \Lambda_{n,\ell}\}}$, $j \neq i$ and $\omega_{i,i} = 1 - \sum_{j \neq i} \omega_{i,j}$, and the additional projection step.

Metrics evaluated (here, $\hat{\mathbb{E}}$ represents a sample average over independent realizations of network deployment, AWGN noise and fading): {1} the *total error* $\frac{1}{\|\mathbf{w}^*\|} \sqrt{\frac{1}{N} \sum_i \hat{\mathbb{E}}[\|\mathbf{w}_{i,k} - \mathbf{w}^*\|^2]}$, measuring the distance between the local optimization variables $\mathbf{w}_{i,k}$ and the global optimum \mathbf{w}^* ; this is further split into {2} the *consensus error* $\frac{1}{\|\mathbf{w}^*\|} \sqrt{\frac{1}{N} \sum_i \hat{\mathbb{E}}[\|\mathbf{w}_{i,k} - \bar{\mathbf{w}}_k\|^2]}$, measuring the distance between $\mathbf{w}_{i,k}$ and the network average $\bar{\mathbf{w}}_k$, and {3} the *optimality error* $\frac{1}{\|\mathbf{w}^*\|} \sqrt{\hat{\mathbb{E}}[\|\bar{\mathbf{w}}_k - \mathbf{w}^*\|^2]}$, measuring the distance between the network average and the global optimum;⁴ {4} the gap $\hat{\mathbb{E}}[F(\bar{\mathbf{w}}_k) - F(\mathbf{w}^*)]$ between the loss evaluated at the network average and the global optimum; {5} the *test error rate* (TER) $\hat{\mathbb{E}}[\frac{1}{N} \sum_i \text{TER}_{i,k}]$, evaluated on a test set of 1000 data points (100 of each digit), averaged over the network, where $\text{TER}_{i,k}$ is the test error rate of node i at time k . For a parameter vector $\mathbf{w}^\top = [\mathbf{w}^{(1)\top}, \dots, \mathbf{w}^{(9)\top}] \in \mathbb{R}^d$ and $\mathbf{w}^{(0)} = \mathbf{0}_{100}$, we predict the label associated to feature vector \mathbf{d} as $\hat{\ell} = \arg \max_{\ell=0,\dots,9} \mathbf{d}^\top \cdot \mathbf{w}^{(\ell)}$.

Discussion: In Fig. 1a, we evaluate the total error versus number of nodes N , reached after a running time of 2000ms (legend shown in Fig. 1b). We also plot the “noiseless” versions of each algorithm, obtained via (1) for OD- and OA-DSGD and (8) for NCOTA-DSGD, with full-batch gradient computations, using the mixing weights of each respective algorithm. We plot two variants of OD-DSGD, to demonstrate the impact of noise propagation: the one described earlier, and an “error-resilient” variant with 1% (instead of 10%) target outage probability for nodes within 500m radius of the transmitter and 25 (instead of 5) quantization levels per scalar. Remarkably, NCOTA-DSGD performs nearly identically as N is varied, and outperforms all other schemes when $N \geq 200$. In fact, in this regime, OD/OA-DSGD have large frame durations, hence can only accomplish a few iterations within the 2000ms target time. In contrast, the frame duration of NCOTA-DSGD is 1.8ms (> 1000 iterations) irrespective of N . We also notice that NCOTA-DSGD is robust to errors (it closely matches the total error of the respective noiseless version), due to the use of a consensus stepsize. Comparing the two variants of OD-DSGD, the error-resilient version outperforms its variant for $N \leq 60$, thanks to less likely channel outage and more precise quantization, and severe error propagation of the baseline (as seen by the gap with respect to its noise-free variant). On the other hand, the baseline variant is preferable

⁴Note that $[\text{total error}] = \sqrt{[\text{consensus error}]^2 + [\text{optimality error}]^2}$

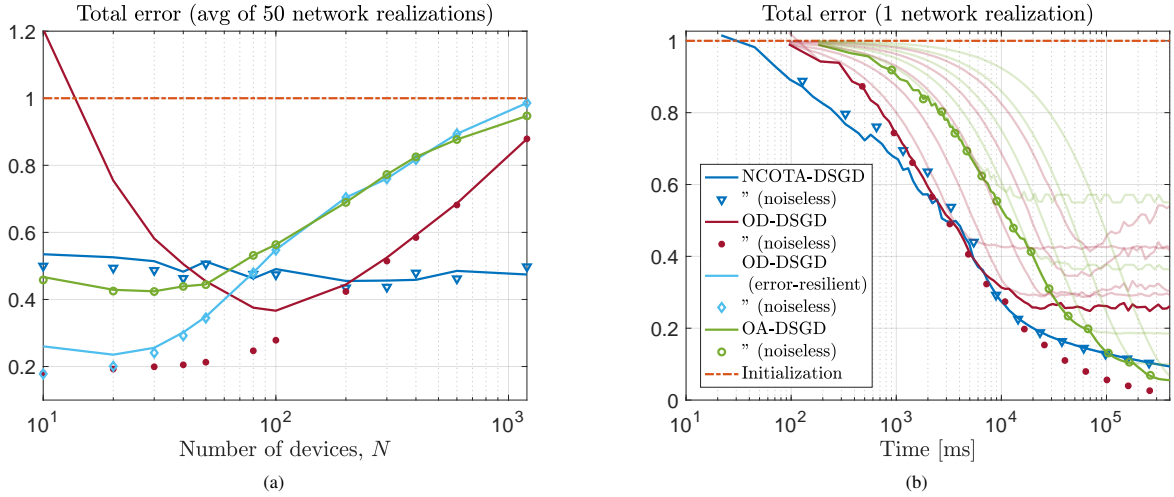


Fig. 1: (a) Total error vs number of nodes N , for a target time of 2000ms. (b) Total error over a long run, for $N = 400$ nodes: the semi-transparent curves for OD/OA-DSGD represent different stepsize choices, whereas the dark ones are evaluated on the best performing stepsize (for each point in the x -axis).

when $N > 60$: its shorter frame duration ($\approx 1/3$ of the error resilient variant) outweighs the impact of noise propagation. In the subsequent evaluations, we focus on $N = 400$ nodes (3 datapoints per node, 3km deployment radius), hence evaluate only the best performing baseline variant of OD-DSGD.

In Fig. 1b, we plot the total error versus time, up to 400s. The total error of NCOTA-DSGD decreases over time, thanks to the use of decreasing consensus and learning stepsizes. In contrast, OD/OA-DSGD reach an error floor, mitigated via smaller stepsizes. Generally, NCOTA-DSGD achieves the best performance across the entire time range thanks to its much faster updates: its frame duration is a fraction $\approx 1/53$ of OD-DSGD and $\approx 1/100$ of OA-DSGD. The better performance of OA-DSGD after 100s is attributed to the fact that, when approaching \mathbf{w}^* , errors become more harmful to the convergence: OA-DSGD is less impacted by fading than NCOTA-DSGD, since it estimates the channels and coherently combines the signals, at the cost of a longer frame duration to orthogonalize transmissions.

In Fig. 2, we plot the 5 performance metrics over a time interval of 2000ms, averaged over 50 independent realizations of network deployment, fading, AWGN noise (OD/OA-DSGD are evaluated with the best stepsize, optimized numerically). The shaded region represent the standard deviation across these realizations (and across the nodes in the network for the test error). Note that this time interval corresponds to 1110 iterations of NCOTA-DSGD, but only 21 of OD-DSGD and 11 of OA-DSGD. During this time, NCOTA-DSGD converges the fastest across all metrics, demonstrating that it is a competitive strategy under stringent delay constraints. However, NCOTA-DSGD exhibits wider performance variations (larger standard deviation) across the 50 independent realizations, due to the harsher impact of fading on its performance.

V. CONCLUSIONS

We presented NCOTA-DSGD, a decentralized SGD algorithm that combines local stochastic gradient descent with Non-Coherent Over-The-Air consensus at the receivers to

solve distributed machine-learning problems over wirelessly-connected systems. NCOTA-DSGD leverages the waveform superposition properties of the wireless channels to efficiently compute consensus, via preamble-based encoding of the optimization signals, coupled with non-coherent combining of the received signals. We showed that NCOTA-DSGD operates without channel state information and leverages the channel pathloss to mix signals, without explicit knowledge of the mixing weights. We proved that the error of NCOTA-DSGD vanishes with rate $\mathcal{O}(k^{-1/4})$ after k iterations, using suitably tuned consensus and learning stepsizes. Supported by numerical evaluations, we demonstrated that NCOTA-DSGD is a competitive strategy to solve optimization problems over wirelessly-connected networks with large number of devices, and operating under stringent delay constraints.

REFERENCES

- [1] N. Michelusi, "Decentralized federated learning via non-coherent over-the-air consensus," in *IEEE International Conference on Communications (ICC) 2023*, submitted. [Online]. Available: <https://arxiv.org/abs/2210.15806>
- [2] H. B. McMahan, E. Moore, D. Ramage, S. Hampson, and B. A. y Arcas, "Communication-efficient learning of deep networks from decentralized data," in *AISTATS*, 2017.
- [3] X. Lian, C. Zhang, H. Zhang, C.-J. Hsieh, W. Zhang, and J. Liu., "Can decentralized algorithms outperform centralized algorithms? A case study for decentralized parallel stochastic gradient descent," in *Proc. 31st NeurIPS*, Dec. 2017.
- [4] G. Zhu, Y. Wang, and K. Huang, "Broadband analog aggregation for low-latency federated edge learning," *IEEE Transactions on Wireless Communications*, vol. 19, no. 1, pp. 491–506, 2020.
- [5] S. Savazzi, M. Nicoli, and V. Rampa, "Federated learning with cooperating devices: A consensus approach for massive iot networks," *IEEE Internet of Things Journal*, vol. 7, no. 5, pp. 4641–4654, 2020.
- [6] A. Nedić, J.-S. Pang, G. Scutari, and Y. Sun, *Multi-agent Optimization*, 1st ed. Springer, Cham, 2018.
- [7] A. Nedić and A. Ozdaglar, "Distributed subgradient methods for multi-agent optimization," *IEEE Trans. Autom. Control*, vol. 54, no. 1, pp. 48–61, Jan. 2009.
- [8] K. Yuan, Q. Ling, and W. Yin, "On the Convergence of Decentralized Gradient Descent," *SIAM Journal on Optimization*, vol. 26, no. 3, pp. 1835–1854, 2016.
- [9] R. Xin, S. Kar, and U. A. Khan, "Decentralized stochastic first-order methods for large-scale machine learning," *CoRR*, vol. abs/1907.09648, 2019. [Online]. Available: <http://arxiv.org/abs/1907.09648>

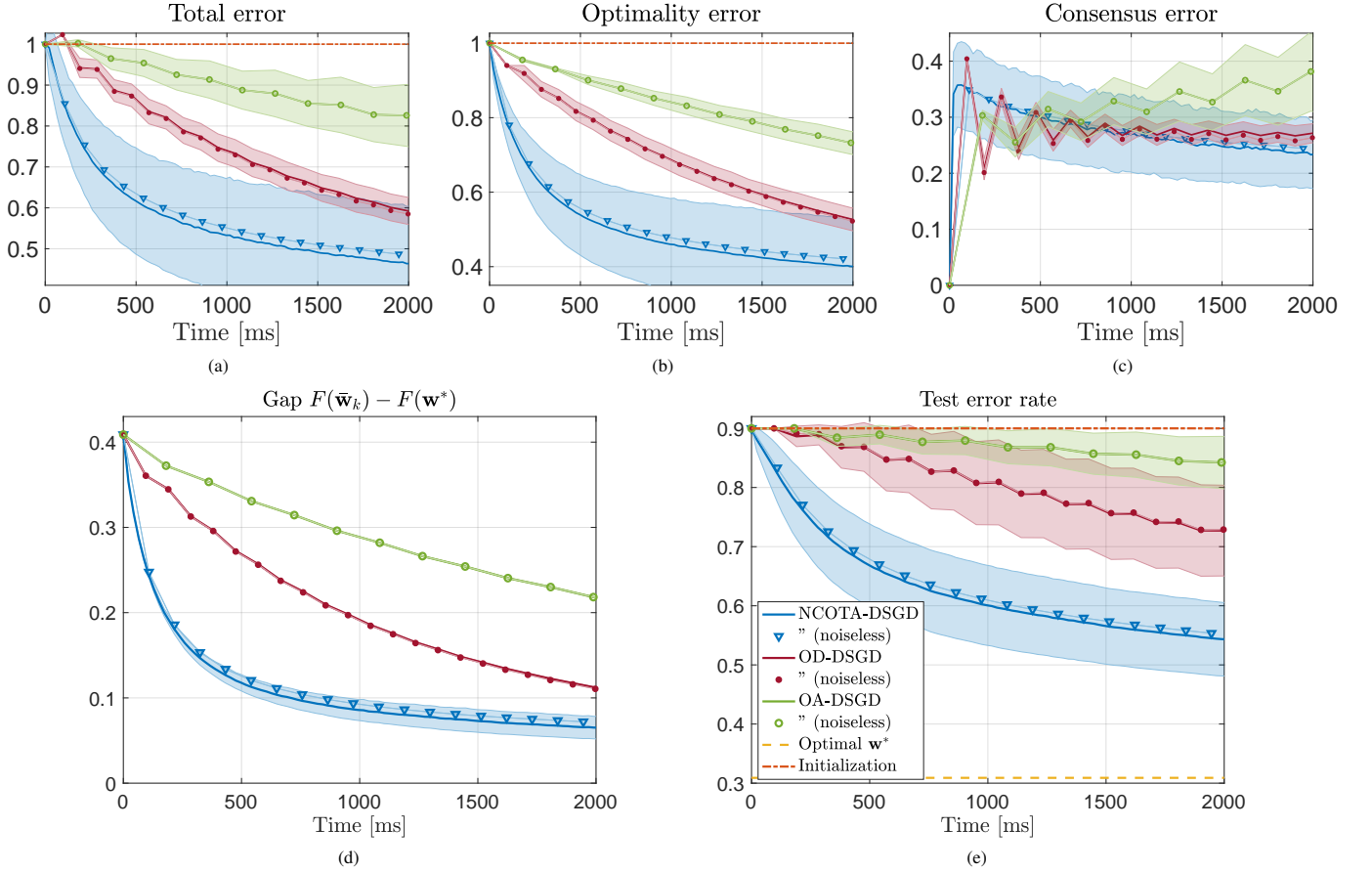


Fig. 2: Performance metrics evaluated over a time interval of 2000ms, averaged over 50 independent realizations of network deployment, fading and noise. The width of the shaded region represents the standard deviation of the respective metrics. Common legend shown in Fig. 2e.

- [10] O. Elijah, C. Y. Leow, T. A. Rahman, S. Nunoo, and S. Z. Iliya, "A comprehensive survey of pilot contamination in massive mimo-5g system," *IEEE Communications Surveys & Tutorials*, vol. 18, no. 2, pp. 905–923, 2016.
- [11] K. Yang, T. Jiang, Y. Shi, and Z. Ding, "Federated learning via over-the-air computation," *IEEE Transactions on Wireless Communications*, vol. 19, no. 3, pp. 2022–2035, 2020.
- [12] M. M. Amiri and D. Gündüz, "Federated learning over wireless fading channels," *IEEE Transactions on Wireless Communications*, vol. 19, no. 5, pp. 3546–3557, 2020.
- [13] M. M. Amiri, D. Gündüz, S. R. Kulkarni, and H. V. Poor, "Convergence of federated learning over a noisy downlink," *IEEE Transactions on Wireless Communications*, vol. 21, no. 3, pp. 1422–1437, 2022.
- [14] G. Zhu, Y. Du, D. Gündüz, and K. Huang, "One-bit over-the-air aggregation for communication-efficient federated edge learning: Design and convergence analysis," *IEEE Transactions on Wireless Communications*, vol. 20, no. 3, pp. 2120–2135, 2021.
- [15] Y. Chen, G. Zhu, and J. Xu, "Over-the-air computation with imperfect channel state information," in *2022 IEEE 23rd International Workshop on Signal Processing Advances in Wireless Communication (SPAWC)*, 2022, pp. 1–5.
- [16] M. M. Amiri, T. M. Duman, D. Gündüz, S. R. Kulkarni, and H. V. Poor, "Blind federated edge learning," *IEEE Transactions on Wireless Communications*, vol. 20, no. 8, pp. 5129–5143, 2021.
- [17] M. Mohammadi Amiri and D. Gündüz, "Machine learning at the wireless edge: Distributed stochastic gradient descent over-the-air," *IEEE Transactions on Signal Processing*, vol. 68, pp. 2155–2169, 2020.
- [18] H. Xing, O. Simeone, and S. Bi, "Federated learning over wireless device-to-device networks: Algorithms and convergence analysis," *IEEE Journal on Selected Areas in Communications*, vol. 39, no. 12, pp. 3723–3741, 2021.
- [19] Y. Shi, Y. Zhou, and Y. Shi, "Over-the-air decentralized federated learning," in *2021 IEEE International Symposium on Information Theory (ISIT)*, 2021, pp. 455–460.
- [20] E. Ozfatura, S. Rini, and D. Gündüz, "Decentralized sgd with over-the-air computation," in *GLOBECOM 2020 - 2020 IEEE Global Communications Conference*, 2020, pp. 1–6.
- [21] J. Choi, "Communication-efficient distributed sgd using random access for over-the-air computation," *IEEE Journal on Selected Areas in Information Theory*, pp. 1–1, 2022.
- [22] J. Tsitsiklis, D. Bertsekas, and M. Athans, "Distributed asynchronous deterministic and stochastic gradient optimization algorithms," *IEEE Transactions on Automatic Control*, vol. 31, no. 9, pp. 803–812, 1986.
- [23] H. Taheri, A. Mokhtari, H. Hassani, and R. Pedarsani, "Quantized decentralized stochastic learning over directed graphs," in *Proc. 37th ICML*, Jul. 2020.
- [24] D. Kovalev, A. Koloskova, M. Jaggi, P. Richtárik, and S. U. Stich, "A linearly convergent algorithm for decentralized optimization: Sending less bits for free!" in *Proc. 24th AISTATS*, Apr. 2021.
- [25] Y. Liao, Z. Li, K. Huang, and S. Pu, "A compressed gradient tracking method for decentralized optimization with linear convergence," *IEEE Transactions on Automatic Control*, vol. 67, no. 10, pp. 5622–5629, 2022.
- [26] N. Michelusi, G. Scutari, and C.-S. Lee, "Finite-bit quantization for distributed algorithms with linear convergence," *IEEE Transactions on Information Theory*, pp. 1–1, 2022.
- [27] Y. Kajiyama, N. Hayashi, and S. Takai, "Linear convergence of consensus-based quantized optimization for smooth and strongly convex cost functions," *IEEE Transactions on Automatic Control*, vol. 66, no. 3, pp. 1254–1261, 2021.
- [28] S. Magnússon, H. Shokri-Ghadikolaei, and N. Li, "On maintaining linear convergence of distributed learning and optimization under limited communication," *IEEE Trans. Signal Process.*, vol. 68, pp. 6101–6116, Oct. 2020.
- [29] R. Saha, S. Rini, M. Rao, and A. J. Goldsmith, "Decentralized optimization over noisy, rate-constrained networks: Achieving consensus by communicating differences," *IEEE Journal on Selected Areas in Communications*, vol. 40, no. 2, pp. 449–467, 2022.
- [30] B. Nazer and M. Gastpar, "Computation over multiple-access channels," *IEEE Transactions on Information Theory*, vol. 53, no. 10, pp. 3498–

- 3516, 2007.
- [31] M. Chen, D. Gündüz, K. Huang, W. Saad, M. Bennis, A. V. Feljan, and H. V. Poor, "Distributed learning in wireless networks: Recent progress and future challenges," *IEEE Journal on Selected Areas in Communications*, vol. 39, no. 12, pp. 3579–3605, 2021.
- [32] V. Gandikota, D. Kane, R. Kumar Maity, and A. Mazumdar, "vqsgd: Vector quantized stochastic gradient descent," in *Proceedings of The 24th International Conference on Artificial Intelligence and Statistics*, vol. 130, 13–15 Apr 2021, pp. 2197–2205.
- [33] C.-S. Lee, N. Michelusi, and G. Scutari, "Finite rate distributed weight-balancing and average consensus over digraphs," *IEEE Transactions on Automatic Control*, vol. 66, no. 10, pp. 4530–4545, 2021.
- [34] M. Chen, H. V. Poor, W. Saad, and S. Cui, "Wireless communications for collaborative federated learning," *IEEE Communications Magazine*, vol. 58, no. 12, pp. 48–54, 2020.
- [35] F. P.-C. Lin, S. Hosseinalipour, S. S. Azam, C. G. Brinton, and N. Michelusi, "Semi-decentralized federated learning with cooperative d2d local model aggregations," *IEEE Journal on Selected Areas in Communications*, vol. 39, no. 12, pp. 3851–3869, 2021.
- [36] M. Yemini, R. Saha, E. Ozfatura, D. Gündüz, and A. J. Goldsmith, "Semi-decentralized federated learning with collaborative relaying," in *2022 IEEE International Symposium on Information Theory (ISIT)*, 2022, pp. 1471–1476.
- [37] S. Hosseinalipour, S. S. Azam, C. G. Brinton, N. Michelusi, V. Agarwal, D. J. Love, and H. Dai, "Multi-stage hybrid federated learning over large-scale d2d-enabled fog networks," *IEEE/ACM Transactions on Networking*, vol. 30, no. 4, pp. 1569–1584, 2022.
- [38] L. Yan, C. Corinna, and C. J. Burges. The MNIST dataset of handwritten digits. [Online]. Available: <http://yann.lecun.com/exdb/mnist/>
- [39] A. H. Sayed, "Adaptation, learning, and optimization over networks," *Foundations and Trends in Machine Learning*, vol. 7, no. 4–5, pp. 311–801, 2014.
- [40] A. Reisizadeh, A. Mokhtari, H. Hassani, and R. Pedarsani, "An exact quantized decentralized gradient descent algorithm," *IEEE Transactions on Signal Processing*, vol. 67, no. 19, pp. 4934–4947, 2019.
- [41] M. Rabbat, "Multi-agent mirror descent for decentralized stochastic optimization," in *IEEE 6th International Workshop on Computational Advances in Multi-Sensor Adaptive Processing (CAMSAP)*, 2015, pp. 517–520.
- [42] J. Wu, W. Hu, H. Xiong, J. Huan, V. Braverman, and Z. Zhu, "On the Noisy Gradient Descent that Generalizes as SGD," in *ICML*, 2020.
- [43] D. Bertsekas, A. Nedić, and A. Ozdaglar, *Convex Analysis and Optimization*. Athena Scientific, 2003.
- [44] Y. Nesterov, *Introductory Lectures on Convex Optimization: A Basic Course*, 1st ed. Springer Publishing Company, Incorporated, 2004.

APPENDIX A: CLOSED-FORM EXPRESSIONS OF $\Sigma^{(1)}$, $\Sigma^{(2)}$

Lemma 1. *Under Rayleigh fading,*

$$\frac{1}{N} \mathbb{E}[\|\epsilon_k^{(1)}\|^2 | \mathcal{F}_k] \leq \left[\Lambda^* + \frac{M(S-1)\sigma^2}{QE} \right] \max_{m,m'} \|\mathbf{z}_m - \mathbf{z}_{m'}\|^2 \triangleq \Sigma^{(1)}$$

Proof. Using (4), we can rewrite $\epsilon_{i,k}^{(1)}$ as

$$\epsilon_{i,k}^{(1)} = \sum_{t \neq \tau_i} \sum_{m=1}^M (|r_{i,m}^{k,t}|^2 - \mathbb{E}[|r_{i,m}^{k,t}|^2 | \mathcal{F}_k]) (\mathbf{z}_m - \mathbf{w}_{i,k}).$$

Noting that $\sqrt{\mathbb{E}[\|\sum_i \mathbf{a}_i\|^2 | \mathcal{F}_k]}$ satisfies the triangle inequality $\leq \sum_i \sqrt{\mathbb{E}[\|\mathbf{a}_i\|^2 | \mathcal{F}_k]}$ (a direct consequence of Cauchy-Schwarz and Holder's inequalities), we bound

$$\sqrt{\mathbb{E}[\|\epsilon_{i,k}^{(1)}\|^2 | \mathcal{F}_k]} \leq \sum_{t \neq \tau_i} \sum_{m=1}^M \text{stdev}(|r_{i,m}^{k,t}|^2 | \mathcal{F}_k) \|\mathbf{z}_m - \mathbf{w}_{i,k}\|,$$

where $\text{stdev}(|r_{i,m}^{k,t}|^2 | \mathcal{F}_k)$ is the standard deviation of $|r_{i,m}^{k,t}|^2$, conditional on \mathcal{F}_k . Since $|r_{i,m}^{k,t}|^2 | \mathcal{F}_k$ is exponentially distributed with mean given by (3), it follows $\text{stdev}(|r_{i,m}^{k,t}|^2 | \mathcal{F}_k) = \mathbb{E}[|r_{i,m}^{k,t}|^2 | \mathcal{F}_k]$. Moreover, $\|\mathbf{z}_m - \mathbf{w}_{i,k}\| =$

$\|\sum_{m'=1}^M [\mathbf{p}_{i,k}]_{m'} (\mathbf{z}_m - \mathbf{z}_{m'})\| \leq \sum_{m'=1}^M [\mathbf{p}_{i,k}]_{m'} \|\mathbf{z}_m - \mathbf{z}_{m'}\| \leq \max_{m,m'} \|\mathbf{z}_m - \mathbf{z}_{m'}\|$. Using (3), it then follows

$$\sqrt{\mathbb{E}[\|\epsilon_{i,k}^{(1)}\|^2 | \mathcal{F}_k]} \leq \left[\sum_{j \in \mathcal{N}_i} \Lambda_{i,j} + \frac{M(S-1)\sigma^2}{QE} \right] \max_{m,m'} \|\mathbf{z}_m - \mathbf{z}_{m'}\|.$$

The result directly follows after using $\sum_{j \in \mathcal{N}_i} \Lambda_{i,j} \leq \Lambda^*$, squaring both sides and adding over i ($\mathbb{E}[\|\epsilon_k^{(1)}\|^2 | \mathcal{F}_k] = \sum_i \mathbb{E}[\|\epsilon_{i,k}^{(1)}\|^2 | \mathcal{F}_k]$). \square

Lemma 2. *Assume $|\mathcal{D}_i| = D \geq 2$, $\forall i$ and minibatch gradient descent is used with minibatch size $|\mathcal{B}_{i,k}| = B \in \{1, \dots, D\}$, $\forall i, k$, with datapoints sampled uniformly at random, without replacement. Assume that: $\{1\}$ the loss function $\phi(\xi; \mathbf{w})$ is strongly-convex and smooth with respect to \mathbf{w} , with parameters μ, L (implying Assumption 1); $\{2\}$ $\|\phi(\xi; \mathbf{w}^*)\| \leq \nabla_{\max}$, $\forall \xi \in \mathcal{D}_i$, $\forall i$ (implying Definition 2). Then,*

$$\frac{1}{N} \mathbb{E}[\|\epsilon_k^{(2)}\|^2 | \mathcal{F}_k] \leq \frac{D-B}{B(D-1)} (\nabla_{\max} + Ld_{\mathcal{W}})^2 \triangleq \Sigma^{(2)}.$$

Proof. The proof directly follows from [42, Prop. 1], along with $\|\phi(\xi; \mathbf{w})\| \leq \|\phi(\xi; \mathbf{w}^*)\| + \|\phi(\xi; \mathbf{w}) - \phi(\xi; \mathbf{w}^*)\| \leq \Delta_{\max} + L\|\mathbf{w} - \mathbf{w}^*\| \leq \Delta_{\max} + Ld_{\mathcal{W}}$. \square

APPENDIX B: PROOF OF THEOREM 1

We prove (17)–(19) in B.I–B.III, using the auxiliary lemmas in B.IV. We let $\mathbf{D} \triangleq \mathbf{I}_{Nd} - \hat{\Omega}$. Since $\hat{\Omega}$ is doubly-stochastic, \mathbf{D} is semidefinite positive ($\mathbf{D} \succeq \mathbf{0}$), $\mathbf{D}(\mathbf{1}_N \otimes \mathbf{z}) = \mathbf{0}_{Nd}$, $\forall \mathbf{z} \in \mathbb{R}^d$, and $\|\mathbf{D}\mathbf{q}\| \geq (1 - \rho_2)\|\mathbf{q}\|$, for any $\mathbf{q} \perp (\mathbf{1}_N \otimes \mathbf{I}_d)$.

Appendix B.I: Proof of (17)

Using the non-expansive property of projections (see, for instance, [43]), we can bound $\|\mathbf{W}_{k+1} - \tilde{\mathbf{W}}_{k+1}\|^2$

$$\leq \|\mathbf{W}_k - \tilde{\mathbf{W}}_k - \eta_k(\nabla G_k(\mathbf{W}_k) - \nabla G_k(\tilde{\mathbf{W}}_k)) + \gamma_k \epsilon_k^{(1)} - \eta_k \epsilon_k^{(2)}\|^2.$$

Taking the expectation conditional on \mathcal{F}_k and using the independence of $\epsilon_k^{(1)}$ and $\epsilon_k^{(2)}$, it follows $\mathbb{E}[\|\mathbf{W}_{k+1} - \tilde{\mathbf{W}}_{k+1}\|^2 | \mathcal{F}_k]$

$$\leq \|(\mathbf{W}_k - \tilde{\mathbf{W}}_k) - \eta_k(\nabla G_k(\mathbf{W}_k) - \nabla G_k(\tilde{\mathbf{W}}_k))\|^2 \quad (30)$$

$$+ \gamma_k^2 N \Sigma^{(1)} + \eta_k^2 N \Sigma^{(2)}. \quad (31)$$

Note that Assumption 1 implies that G_k is μ -strongly convex and $L_{G,k} \triangleq L + \frac{\gamma_k}{\eta_k} \Lambda^*(1 - \rho_N)$ -smooth. Then, using [44, Theorem 2.1.12], (30) $\leq (1 - \mu\eta_k)^2 \|\mathbf{W}_k - \tilde{\mathbf{W}}_k\|^2$, as long as $\eta_k \leq 2/(\mu + L_{G,k})$ i.e. $\eta_k(\mu + L) + \gamma_k \Lambda^*(1 - \rho_N) \leq 2$ (C1 of Theorem 1). Using this bound and computing the unconditional expectation, it follows $\|\mathbf{W}_{k+1} - \tilde{\mathbf{W}}_{k+1}\|_{\mathbb{E}}^2$

$$\leq (1 - \mu\eta_k)^2 \|\mathbf{W}_k - \tilde{\mathbf{W}}_k\|_{\mathbb{E}}^2 + \gamma_k^2 N \Sigma^{(1)} + \eta_k^2 N \Sigma^{(2)}.$$

The result follows by induction and noting that $\mathbf{W}_{\bar{\kappa}} = \tilde{\mathbf{W}}_{\bar{\kappa}}$.

Appendix B.II: Proof of (19)

First, we show that, when $\frac{\eta_k}{\gamma_k} \leq \frac{\zeta \cdot Z}{\sqrt{N} \nabla_{\max}}$ (C2 of Theorem 1), the minimizer of $G_k(\mathbf{W})$, \mathbf{W}_k^* , is such that $\nabla G_k(\mathbf{W}_k^*) = \mathbf{0}_{Nd}$.⁵

⁵This condition may not be true when \mathbf{W}_k^* lies on the boundary of \mathcal{W}^N

To this end, consider the *unconstrained* minimizer⁶

$$\hat{\mathbf{W}}_k \triangleq \arg \min_{\mathbf{W} \in \mathbb{R}^{Nd}} G_k(\mathbf{W}).$$

Note that $\hat{\mathbf{W}}_k$ minimizes G_k over \mathbb{R}^{Nd} , whereas \mathbf{W}_k^* minimizes it over \mathcal{W}^N . Since G_k is strongly-convex and smooth on \mathbb{R}^{Nd} , its minimizer exists and is the unique solution of $\nabla G_k(\hat{\mathbf{W}}_k) = \mathbf{0}_{Nd}$ in \mathbb{R}^{Nd} . We now bound the distance of $\hat{\mathbf{W}}_k$ from $\mathbf{1}_N \otimes \mathbf{w}^*$. Noting that there exists \mathbf{A} positive definite with $\mu \mathbf{I}_{Nd} \preceq \mathbf{A} \preceq L \mathbf{I}_{Nd}$ such that

$$\nabla f(\hat{\mathbf{W}}_k) = \nabla f(\mathbf{1}_N \otimes \mathbf{w}^*) + \mathbf{A}(\hat{\mathbf{W}}_k - \mathbf{1}_N \otimes \mathbf{w}^*),$$

(multivariate mean value theorem) it follows that

$$\begin{aligned} \mathbf{0}_{Nd} &= \nabla G_k(\hat{\mathbf{W}}_k) = \nabla f(\hat{\mathbf{W}}_k) + \frac{\gamma_k}{\eta_k} \Lambda^* \mathbf{D} \hat{\mathbf{W}}_k \\ &= \nabla f(\mathbf{1}_N \otimes \mathbf{w}^*) + \mathbf{B}(\hat{\mathbf{W}}_k - \mathbf{1}_N \otimes \mathbf{w}^*), \end{aligned}$$

where we have defined $\mathbf{B} \triangleq \mathbf{A} + U\mathbf{D} \succeq \mu \mathbf{I}_{Nd}$, $U = \frac{\gamma_k}{\eta_k} \Lambda^*$. Solving with respect to $\hat{\mathbf{W}}_k - \mathbf{1}_N \otimes \mathbf{w}^*$ and computing the norm of both sides, we find

$$\|\hat{\mathbf{W}}_k - \mathbf{1}_N \otimes \mathbf{w}^*\| = \|\mathbf{B}^{-1} \nabla f(\mathbf{1}_N \otimes \mathbf{w}^*)\|. \quad (32)$$

Noting that $\nabla f(\mathbf{1}_N \otimes \mathbf{w}^*) \perp (\mathbf{1}_N \otimes \mathbf{I}_d)$ (in fact, $\sum_i \nabla f_i(\mathbf{w}^*) = \mathbf{0}_d$ from the optimality condition on \mathbf{w}^* , since $\mathbf{w}^* \in \text{int}(\mathcal{W})$), we bound (32) via Lemma 3 in B.IV with $U = \frac{\gamma_k}{\eta_k} \Lambda^*$ as

$$\|\hat{\mathbf{W}}_k - \mathbf{1}_N \otimes \mathbf{w}^*\| = \frac{1}{Z} \frac{\eta_k}{\gamma_k} \|\nabla f(\mathbf{1}_N \otimes \mathbf{w}^*)\|.$$

(Z defined in Theorem 1). Furthermore, from Definition 2, $\|\nabla f(\mathbf{1}_N \otimes \mathbf{w}^*)\| \leq \sqrt{\sum_i \|\nabla f_i(\mathbf{w}^*)\|^2} \leq \sqrt{N} \nabla_{\max}$, yielding

$$\|\hat{\mathbf{W}}_k - \mathbf{1}_N \otimes \mathbf{w}^*\| \leq \frac{\sqrt{N} \Delta_{\max}}{Z} \frac{\eta_k}{\gamma_k}. \quad (33)$$

Next, we show that $\hat{\mathbf{W}}_k \in \mathcal{W}^N$, hence it coincides with the solution of the constrained problem, so that $\hat{\mathbf{W}}_k = \mathbf{W}_k^*$. Indeed, \mathbf{w}^* is at distance ζ from the boundary of \mathcal{W} (Assumption 2). It then suffices to show that $\|\hat{\mathbf{w}}_{i,k} - \mathbf{w}^*\| \leq \zeta$, $\forall i$ (i.e., \mathbf{w}^* is closer to $\hat{\mathbf{w}}_{i,k}$ than to the boundary of \mathcal{W}). Indeed, $\|\hat{\mathbf{w}}_{i,k} - \mathbf{w}^*\| \leq \|\hat{\mathbf{W}}_k - \mathbf{1}_N \otimes \mathbf{w}^*\| \leq \frac{\sqrt{N} \Delta_{\max}}{Z} \frac{\eta_k}{\gamma_k}$, hence, when $\frac{\eta_k}{\gamma_k} \leq \frac{\zeta \cdot Z}{\sqrt{N} \Delta_{\max}}$ (C2 of Theorem 1), $\hat{\mathbf{W}}_k = \mathbf{W}_k^*$,

$$\nabla G_k(\mathbf{W}_k^*) = \mathbf{0}_{Nd}, \quad (34)$$

and (19) readily follows from (33).

Appendix B.III: Proof of (18)

Using the triangle inequality, we bound

$$\|\tilde{\mathbf{W}}_{k+1} - \mathbf{W}_{k+1}^*\| \leq \|\tilde{\mathbf{W}}_{k+1} - \mathbf{W}_k^*\| + \|\mathbf{W}_{k+1}^* - \mathbf{W}_k^*\|. \quad (35)$$

Using the fixed point optimality condition $\mathbf{W}_k^* = \Pi^N[\mathbf{W}_k^* - \eta \nabla G_k(\mathbf{W}_k^*)]$, $\forall \eta \geq 0$ and the non-expansive property of

projections [43], we bound the first term of (35) as

$$\begin{aligned} \|\tilde{\mathbf{W}}_{k+1} - \mathbf{W}_k^*\| &= \left\| \Pi^N[\tilde{\mathbf{W}}_k - \eta_k \nabla G_k(\tilde{\mathbf{W}}_k)] \right. \\ &\quad \left. - \Pi^N[\mathbf{W}_k^* - \eta_k \nabla G_k(\mathbf{W}_k^*)] \right\| \\ &\leq \left\| \tilde{\mathbf{W}}_k - \mathbf{W}_k^* - \eta_k (\nabla G_k(\tilde{\mathbf{W}}_k) - \nabla G_k(\mathbf{W}_k^*)) \right\| \\ &\leq (1 - \mu \eta_k) \|\tilde{\mathbf{W}}_k - \mathbf{W}_k^*\|, \end{aligned} \quad (36)$$

where in the last step we used [44, Theorem 2.1.12] since G_k is μ -strongly convex and $L_{G,k} \triangleq L + \frac{\gamma_k}{\eta_k} \Lambda^* (1 - \rho_N)$ -smooth, provided that $\eta_k \leq 2/(\mu + L_{G,k})$ (C1 of Theorem 1). We now bound $\|\mathbf{W}_{k+1}^* - \mathbf{W}_k^*\|$. First, note that, for $\ell \geq \bar{\kappa}$, \mathbf{W}_ℓ^* satisfies the optimality condition $\nabla G_\ell(\mathbf{W}_\ell^*) = \mathbf{0}_{Nd}$, $\forall \ell \geq \bar{\kappa}$ (see (34)). It then follows that

$$\mathbf{0}_{Nd} = \nabla G_{k+1}(\mathbf{W}_{k+1}^*) = \nabla f(\mathbf{W}_{k+1}^*) + \frac{\gamma_{k+1}}{\eta_{k+1}} \Lambda^* \mathbf{D} \mathbf{W}_{k+1}^*, \quad (37)$$

$$\mathbf{0}_{Nd} = \nabla G_k(\mathbf{W}_k^*) = \nabla f(\mathbf{W}_k^*) + \frac{\gamma_k}{\eta_k} \Lambda^* \mathbf{D} \mathbf{W}_k^*. \quad (38)$$

Furthermore, there exists positive definite \mathbf{A} with $\mu \mathbf{I}_{Nd} \preceq \mathbf{A} \preceq L \mathbf{I}_{Nd}$ such that $\nabla f(\mathbf{W}_{k+1}^*) = \nabla f(\mathbf{W}_k^*) + \mathbf{A}(\mathbf{W}_{k+1}^* - \mathbf{W}_k^*)$ (from the multivariate mean value theorem, and the fact that the Hessian of f satisfies $\mu \mathbf{I}_{Nd} \preceq \nabla^2 f(\mathbf{W}) \preceq L \mathbf{I}_{Nd}$). Using this expression in (37) along with $\nabla f(\mathbf{W}_k^*)$ from (38), reorganizing and solving with respect to $\mathbf{W}_{k+1}^* - \mathbf{W}_k^*$, yields

$$\mathbf{W}_{k+1}^* - \mathbf{W}_k^* = -\Lambda^* \left(\frac{\gamma_{k+1}}{\eta_{k+1}} - \frac{\gamma_k}{\eta_k} \right) \mathbf{B}^{-1} \mathbf{D} \mathbf{W}_{k+1}^*,$$

where $\mathbf{B} \triangleq \mathbf{A} + U\mathbf{D}$, $U = \frac{\gamma_k}{\eta_k} \Lambda^*$. Therefore,

$$\|\mathbf{W}_{k+1}^* - \mathbf{W}_k^*\| \leq \Lambda^* \left(\frac{\gamma_{k+1}}{\eta_{k+1}} - \frac{\gamma_k}{\eta_k} \right) \|\mathbf{B}^{-1} \mathbf{D} \mathbf{W}_{k+1}^*\|. \quad (39)$$

Noting that $\mathbf{D} \mathbf{W}_{k+1}^* \perp (\mathbf{1}_N \otimes \mathbf{I}_d)$, we use Lemma 3 in B.IV with $U = \frac{\gamma_k}{\eta_k} \Lambda^*$ to bound

$$\|\mathbf{W}_{k+1}^* - \mathbf{W}_k^*\| \leq \frac{2\sqrt{1+L/\mu}}{1-\rho_2} \left(\frac{\gamma_{k+1}}{\eta_{k+1}} - \frac{\gamma_k}{\eta_k} \right) \frac{\eta_k}{\gamma_k} \|\mathbf{D} \mathbf{W}_{k+1}^*\|.$$

Using Lemma 4 in B.IV and the fact that $\frac{\eta_{k+1}}{\gamma_{k+1}} \leq \frac{\eta_k}{\gamma_k}$ (C3 of Theorem 1), we further bound

$$\|\mathbf{D} \mathbf{W}_{k+1}^*\| \leq \frac{\sqrt{N} (\nabla_{\max} + L d_{\mathcal{W}})}{\Lambda^*} \frac{\eta_k}{\gamma_k}; \quad (40)$$

combining this result with the previous inequality yields

$$\|\mathbf{W}_{k+1}^* - \mathbf{W}_k^*\| \leq \frac{\sqrt{N} (\nabla_{\max} + L d_{\mathcal{W}})}{Z} \left(\frac{\gamma_{k+1}}{\eta_{k+1}} - \frac{\gamma_k}{\eta_k} \right) \frac{\eta_k^2}{\gamma_k^2}. \quad (41)$$

We obtain the final result (18) by combining this result with (36) into (35), solving via induction, and noting that

$$\|\tilde{\mathbf{W}}_{\bar{\kappa}} - \mathbf{W}_{\bar{\kappa}}^*\| = \sqrt{\sum_i \|\tilde{\mathbf{w}}_{i,\bar{\kappa}} - \mathbf{w}_{i,\bar{\kappa}}^*\|^2} \leq \sqrt{N} d_{\mathcal{W}}.$$

Appendix B.IV: Auxiliary lemmas

Lemma 3. Let $\mathbf{B} = \mathbf{A} + U\mathbf{D}$, where $U > 0$, $\mu \mathbf{I}_{Nd} \preceq \mathbf{A} \preceq L \mathbf{I}_{Nd}$. Then, for any $\mathbf{v} \in \mathbb{R}^{Nd}$ with $\mathbf{v} \perp (\mathbf{1}_N \otimes \mathbf{I}_d)$,

$$\|\mathbf{B}^{-1} \mathbf{v}\| \leq \frac{2\sqrt{1+L/\mu}}{U(1-\rho_2)} \|\mathbf{v}\|.$$

⁶Here, we assume that all f_i 's are defined on \mathbb{R}^d , and the extended functions are L -smooth and μ -strongly convex on \mathbb{R}^d

Proof. Consider $\mathbf{v} \neq \mathbf{0}_{Nd}$ (the result holds trivially for $\mathbf{v} = \mathbf{0}_{Nd}$). We use the change of variables $\mathbf{B}^{-1}\mathbf{v} = \mathbf{1}_N \otimes \mathbf{z} + \mathbf{q}$ where $\mathbf{z} \in \mathbb{R}^d$ and $\mathbf{q} \perp (\mathbf{1}_N \otimes \mathbf{I}_d)$. Noting that $\mathbf{v} = \mathbf{B}(\mathbf{1}_N \otimes \mathbf{z} + \mathbf{q}) = \mathbf{A}(\mathbf{1}_N \otimes \mathbf{z} + \mathbf{q}) + U\mathbf{D}\mathbf{q}$, and using the fact that $\mathbf{v} \perp (\mathbf{1}_N \otimes \mathbf{I}_d)$ (i.e., $(\mathbf{1}_N \otimes \mathbf{z})^\top \mathbf{v} = 0$) and $(\mathbf{1}_N \otimes \mathbf{z})^\top \mathbf{D} = \mathbf{0}$, we obtain using Cauchy-Schwarz inequality

$$\begin{aligned} 0 &= (\mathbf{1}_N \otimes \mathbf{z})^\top \mathbf{v} = (\mathbf{1}_N \otimes \mathbf{z})^\top \mathbf{A}(\mathbf{1}_N \otimes \mathbf{z}) + (\mathbf{1}_N \otimes \mathbf{z})^\top \mathbf{A}\mathbf{q} \\ &\geq \sqrt{(\mathbf{1}_N \otimes \mathbf{z})^\top \mathbf{A}(\mathbf{1}_N \otimes \mathbf{z})} \\ &\quad \times \left(\sqrt{(\mathbf{1}_N \otimes \mathbf{z})^\top \mathbf{A}(\mathbf{1}_N \otimes \mathbf{z})} - \sqrt{\mathbf{q}^\top \mathbf{A}\mathbf{q}} \right). \end{aligned} \quad (42)$$

Since $\mu\mathbf{I}_{Nd} \preceq \mathbf{A} \preceq L\mathbf{I}_{Nd}$, it follows $\sqrt{(\mathbf{1}_N \otimes \mathbf{z})^\top \mathbf{A}(\mathbf{1}_N \otimes \mathbf{z})} \geq \sqrt{\mu N} \|\mathbf{z}\|$ and $\sqrt{\mathbf{q}^\top \mathbf{A}\mathbf{q}} \leq \sqrt{L} \|\mathbf{q}\|$, hence (42) implies $\sqrt{N} \|\mathbf{z}\| \leq \sqrt{L/\mu} \|\mathbf{q}\|$. Using this change of variables over the feasible set $\mathcal{ZQ} \equiv \{(\mathbf{z} \in \mathbb{R}^d, \mathbf{q} \in \mathbb{R}^{Nd}) : \mathbf{q} \perp (\mathbf{1}_N \otimes \mathbf{I}_d), \sqrt{N} \|\mathbf{z}\| \leq \sqrt{L/\mu} \|\mathbf{q}\|\}$, it follows that

$$\begin{aligned} \frac{\|\mathbf{B}^{-1}\mathbf{v}\|}{\|\mathbf{v}\|} &\leq \max_{(\mathbf{z}, \mathbf{q}) \in \mathcal{ZQ}} \frac{\|\mathbf{1}_N \otimes \mathbf{z} + \mathbf{q}\|}{\|\mathbf{B}(\mathbf{1}_N \otimes \mathbf{z} + \mathbf{q})\|} \\ &\leq \max_{(\mathbf{z}, \mathbf{q}) \in \mathcal{ZQ}} \frac{\sqrt{1 + L/\mu} \|\mathbf{q}\|}{\|\mathbf{B}(\mathbf{1}_N \otimes \mathbf{z} + \mathbf{q})\|}, \end{aligned} \quad (43)$$

where we used $\sqrt{N} \|\mathbf{z}\| \leq \sqrt{L/\mu} \|\mathbf{q}\|$ and $(\mathbf{1}_N \otimes \mathbf{z})^\top \mathbf{q} = 0$. We further bound $\|\mathbf{B}(\mathbf{1}_N \otimes \mathbf{z} + \mathbf{q})\|$ as

$$\begin{aligned} \|\mathbf{B}(\mathbf{1}_N \otimes \mathbf{z} + \mathbf{q})\| &\geq U\|\mathbf{D}\mathbf{q}\| - \|\mathbf{A}(\mathbf{1}_N \otimes \mathbf{z} + \mathbf{q})\| \\ &\geq U(1 - \rho_2)\|\mathbf{q}\| - \|\mathbf{A}(\mathbf{1}_N \otimes \mathbf{z} + \mathbf{q})\|. \end{aligned}$$

At the same time, $\mathbf{B} \succeq \mathbf{A} \succeq \mu\mathbf{I}$ implies $\|\mathbf{B}(\mathbf{1}_N \otimes \mathbf{z} + \mathbf{q})\| \geq \|\mathbf{A}(\mathbf{1}_N \otimes \mathbf{z} + \mathbf{q})\|$, hence $\|\mathbf{B}(\mathbf{1}_N \otimes \mathbf{z} + \mathbf{q})\|$

$$\begin{aligned} &\geq \max\{\|\mathbf{A}(\mathbf{1}_N \otimes \mathbf{z} + \mathbf{q})\|, U(1 - \rho_2)\|\mathbf{q}\| - \|\mathbf{A}(\mathbf{1}_N \otimes \mathbf{z} + \mathbf{q})\|\} \\ &\geq \frac{U}{2}(1 - \rho_2)\|\mathbf{q}\|, \end{aligned}$$

after noting that $\max\{a, b\} \geq (a + b)/2$. The result follows after using this bound in (43). \square

Lemma 4. $\|\mathbf{D}\mathbf{W}_k^*\| \leq \frac{\sqrt{N}(\nabla_{\max} + Ld_{\mathcal{W}})}{\Lambda^*} \frac{\eta_k}{\gamma_k}, \forall k$.

Proof. Since $\mathbf{w}_{j,k}^* \in \mathcal{W}, \forall j$, it follows that $\sum_j \omega_{i,j} \mathbf{w}_{j,k}^* \in \mathcal{W}$ (from convexity of \mathcal{W}), hence $\hat{\Omega} \mathbf{W}_k^* \in \mathcal{W}^N$. Therefore, $\nabla G_k(\mathbf{W}_k^*)^\top (\hat{\Omega} \mathbf{W}_k^* - \mathbf{W}_k^*) \geq 0$ (optimality condition), i.e.,

$$\begin{aligned} \nabla f(\mathbf{W}_k^*)^\top (\hat{\Omega} - \mathbf{I}_{Nd}) \mathbf{W}_k^* &= -\nabla f(\mathbf{W}_k^*)^\top \mathbf{D}\mathbf{W}_k^* \\ &\geq \frac{\gamma_k}{\eta_k} \Lambda^* (\mathbf{W}_k^*)^\top \mathbf{D}^2 \mathbf{W}_k^* = \frac{\gamma_k}{\eta_k} \Lambda^* \|\mathbf{D}\mathbf{W}_k^*\|^2. \end{aligned} \quad (44)$$

We also upper bound the left hand side via Cauchy-Schwarz inequality as

$$\begin{aligned} -\nabla f(\mathbf{W}_k^*)^\top \mathbf{D}\mathbf{W}_k^* &\leq \|\nabla f(\mathbf{W}_k^*)\| \|\mathbf{D}\mathbf{W}_k^*\| \\ &\leq \sqrt{N}(\nabla_{\max} + Ld_{\mathcal{W}}) \|\mathbf{D}\mathbf{W}_k^*\|. \end{aligned}$$

where in the last step we used

$$\|\nabla f_i(\mathbf{w}_{i,k}^*)\| \leq \|\nabla f_i(\mathbf{w}^*)\| + L\|\mathbf{w}_{i,k}^* - \mathbf{w}^*\| \leq \nabla_{\max} + Ld_{\mathcal{W}}.$$

The result follows after combining it with (44) and solving with respect to $\|\mathbf{D}\mathbf{W}_k^*\|$. \square

APPENDIX C: PROOF OF THEOREM 2

Proof. Consider $k \geq \bar{k}$ (C1-C3 satisfied). In the proof, we will often need the sum

$$S_k^n(v) \triangleq \delta \sum_{\ell=\bar{k}}^{k-1} P_{\ell+1,k}^n (\ell + \delta)^{-v}, \text{ for } 1 \leq v \leq \frac{5}{4}n \text{ and } n \geq 1.$$

$$\begin{aligned} \text{Using } P_{\ell,k} &= \prod_{j=\ell}^{k-1} (1 - \mu\eta_j) \leq e^{-\mu\eta_0 \delta \sum_{j=\ell}^{k-1} (j+\delta)^{-1}} \\ &\leq e^{-\mu\eta_0 \delta \int_{\ell}^k (x+\delta)^{-1} dx} = (k + \delta)^{-\mu\eta_0 \delta} (\ell + \delta)^{\mu\eta_0 \delta}, \end{aligned}$$

we can bound

$$S_k^n(v) \leq \delta(k + \delta)^{-n\mu\eta_0 \delta} (1 + 1/(\bar{k} + \delta))^{n\mu\eta_0 \delta} \sum_{\ell=\bar{k}}^{k-1} (\ell + \delta)^{n\mu\eta_0 \delta - v}$$

and since $n\mu\eta_0 \delta \geq 5/4n \geq v$ and $(1 + 1/(\bar{k} + \delta))^{n\mu\eta_0 \delta} \leq e^{n\mu\eta_0 \delta / (\bar{k} + \delta)} = e^{n\mu\eta_{\bar{k}}} \leq e^n$ (note that $\eta_{\bar{k}} \leq 2/(\mu + L) \leq 1/\mu$ from C1 of Theorem 1), we proceed as

$$\begin{aligned} S_k^n(v) &\leq \delta(k + \delta)^{-n\mu\eta_0 \delta} e^n \int_{\bar{k}}^k (x + \delta)^{n\mu\eta_0 \delta - v} dx \\ &\leq \frac{e^n \delta}{n\mu\eta_0 \delta - v + 1} (k + \delta)^{-v+1} \leq e^n \frac{5}{4\mu\eta_0} (k + \delta)^{-v+1}, \end{aligned} \quad (45)$$

where the last step used $\delta \geq \frac{5}{4\mu\eta_0}$, $v \leq 5/4n$. With γ_k, η_k as in Theorem 2, we specialize (17) as

$$\begin{aligned} \frac{1}{N} \|\mathbf{W}_k - \tilde{\mathbf{W}}_k\|_{\mathbb{E}}^2 &\leq \sum_{\ell=\bar{k}}^{k-1} P_{\ell+1,k}^2 \left[\gamma_0^2 \delta^{3/2} (\ell + \delta)^{-3/2} \Sigma^{(1)} \right. \\ &\quad \left. + \eta_0^2 \delta^2 (\ell + \delta)^{-2} \Sigma^{(2)} \right] \\ &= \gamma_0^2 \delta^{1/2} \Sigma^{(1)} S_k^2(3/2) + \eta_0^2 \delta \Sigma^{(2)} S_k^2(2); \end{aligned}$$

(24) follows using (45) and $\sqrt{a+b} \leq \sqrt{a} + \sqrt{b}$ for $a, b \geq 0$. Similarly, we specialize (18) as

$$\begin{aligned} \frac{1}{\sqrt{N}} \|\tilde{\mathbf{W}}_k - \mathbf{W}_k^*\|_{\mathbb{E}} &\leq d_{\mathcal{W}} P_{\bar{k},k} + \frac{\nabla_{\max} + Ld_{\mathcal{W}}}{Z} \frac{\eta_0}{\gamma_0} \delta^{1/4} \\ &\quad \times \sum_{\ell=\bar{k}}^{k-1} P_{\ell+1,k} \left((\ell + 1 + \delta)^{1/4} - (\ell + \delta)^{1/4} \right) (\ell + \delta)^{-1/2}. \end{aligned}$$

Since $x^{1/4}$ is concave for $x > 0$, we further bound $(\ell + 1 + \delta)^{1/4} \leq (\ell + \delta)^{1/4} + 1/4(\ell + \delta)^{-3/4}$, hence

$$\begin{aligned} \frac{1}{\sqrt{N}} \|\tilde{\mathbf{W}}_k - \mathbf{W}_k^*\|_{\mathbb{E}} &\leq d_{\mathcal{W}} (\bar{k} + \delta)^{\mu\eta_0 \delta} (k + \delta)^{-\mu\eta_0 \delta} \\ &\quad + \frac{\nabla_{\max} + Ld_{\mathcal{W}}}{4Z} \frac{\eta_0}{\gamma_0} \delta^{-3/4} S_k^1(5/4); \end{aligned}$$

(25) readily follows using (45) and $\delta \geq \frac{5}{4\mu\eta_0}$. (26) follows by direct substitution into (19). \square